DENSITY FUNCTIONAL STUDY OF MECHANICAL, ELECTRONIC AND PRESSURE INDUCED PHASE TRANSITION PROPERTIES OF CALCIUM DIIRON DIARSENIDE, CaFe$_2$As$_2$

MOCHAMA VICTOR SAMUEL

BACHELOR OF EDUCATION SCIENCE (KISII UNIVERSITY)

A THESIS SUBMITTED TO THE BOARD OF POST-GRADUATE STUDIES IN PARTIAL FULFILMENT OF THE REQUIREMENTS FOR THE AWARD OF THE DEGREE OF MASTER OF SCIENCE IN PHYSICS IN THE SCHOOL OF PURE AND APPLIED SCIENCES, DEPARTMENT OF PHYSICS,

KISII UNIVERSITY

2023

DECLARATION AND RECOMMENDATIONS

DECLARATION BY THE CANDIDATE

This research thesis is my original work prepared with no other than the indicated sources and support and has not been presented elsewhere for a degree or any other award.

Name Mochama Victor Samuel **Admission Number** MPS21/00002/20

Signature: …………………….. Date: ……………………..

DECLARATION BY THE SUPERVISORS

This thesis has undergone the due process of review and we hereby recommend it to be accepted in partial fulfillment for the award of the Master degree of science in Physics.

Dr. Calford Otieno

Department of Physics

Kisii University

Sign: _____ Date; ……………………………

Dr. Philip Otieno Nyawere

Department of Physical and Biological Sciences

Kabarak University

Sign: _____ Date: ……………………………..

PLAGIARISM DECLARATION

DECLARATION BY STUDENT

i.   I have read and understood Kisii University Post-graduate Examination Rules and Regulations and other documents concerning academic dishonesty.

ii. I do understand that ignorance of these rules and regulations is not an excuse for a violation of the said rules.

iii. I must keep seeking an answer if I have any question or doubt until I understand.

iv. I understand I must do my work.

v.   I also understand that if I commit any act of academic dishonesty like plagiarism, my thesis/project can be assigned a 'fail' grade ('F')

vi. I understand that I may be suspended or expelled from the University for Academic Dishonesty.

Name: **MOCHAMA VICTOR SAMUEL**   Signature:…………………………
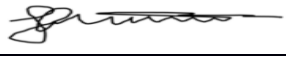
Reg. No: **MPS21/00002/20**   Date: **………………………….**

DECLARATION BY SUPERVISOR (S)

i.   We declare that this thesis has been submitted to the plagiarism detection service.

ii. The thesis/project contains less than 20% of plagiarized work.

iii. We, as a result of this, give consent for marking.

1. **Name: Dr. Calford Otieno**   **Signature;** _____

   Affiliation: Kisii University   **Date;** …………………………………

2. **Name: Dr. Phillip W.O. Nyawere**   **Signature:** _____

   Affiliation: Kabarak University   **Date:**…………………………………..

DECLARATION OF THE NUMBER OF WORDS FOR MASTERS THESIS

This form should be signed by the candidate and the candidate's supervisor (s) and returned to Director of Postgraduate Studies at the same time as your copies of thesis/project. Please note at Kisii University Masters and PhD thesis shall comprise a piece of scholarly writing of more than 20,000 words for the Master's degree and 50,000 words for PhD degree. In both cases this length includes references, but excludes the bibliography and any appendices. Where a candidate wishes to exceed or reduce the word limit for the thesis specified in the regulations, the candidate must enquire with the Director of Postgraduate about the procedures to be followed. Any such enquiries must be made at least 2 months before the submission of the thesis. Please note in cases where students exceed/reduce the prescribed word limit set out, Director of Postgraduate may refer the thesis for resubmission requiring it to be shortened.

I confirm that the word length of:

1) The thesis, including footnotes, is 20,615, 2) the appendices are………………

I also declare the electronic version is identical to the final, hard-bound copy of the thesis and

corresponds with those on which the examiners based their recommendation for the award of the

degree.

Name of Candidate: **Mochama Victor Samuel**   ADM NO: **MPS21/00002/20**

Faculty: Pure and Applied Sciences   Department: Physics

Thesis Title:………………………………………………………………………………..
I confirm that the thesis submitted by the above named candidate complies with the relevant

word length specified in the School of Postgraduate and Commission for University Education

regulations for the Masters and PhD Degrees.

Signed:_____ Tel ……………… Date:…………………..

(Supervisor 1)

Signed:_____ Tel …………………… Date:…………………..

(Supervisor 2)

DEDICATION

I wish to dedicate this dissertation work to my immediate family; my Dad, Samuel Mochama, Mom Anne Samuel and. My brothers, Onesimus, Gideon, and Elijah and my sister Esther for believing in me and always being present for me at all times and encouraged me a lot. A special feeling of gratitude to my relatives, for instance, Nehemiah Tom and his family, for the support received this far. I'm also dedicating this dissertation to my church family, the Kisii Town P.A.G., and friends who have supported me throughout the process. I will always appreciate all they did.

I dedicate this work with special gratitude to my best friend, Sharon Gichana, for reminding me of all I needed to do throughout the entire Master's program. She has been my best cheerleader.

ACKNOWLEDGEMENT

TABLE OF CONTENTS

ABSTRACT

Compounds belonging to the 122 iron pnictide have a $ThCr_2Si_2$ structure with a space group of 14/mmm containing divalent alkali earth metal elements. This study applies First Principle Calculation to investigate mechanical, electronic and structural phase transition properties. The compound has a low value of Vicker hardness an indication that it is not strong enough to resist being dented. This property enables them suitable for the use as bake hardeners which provide a good formability before stamping and enhance strength post baking. It has low value of Debye temperature hence frozen high frequency modes are expected that enhances field amplitude which can be very attractive in various applications such as dispersion engineering, lasers and delay lines. The compound is metallic. The compound has phase transition from the stable phase non-superconducting tetragonal to type I orthorhombic superconducting phase. This plays a big role in enhancing conductivity. We are making use of the Quantum Espresso simulation package which is a suite for First Principles electronic structure calculations and material modelling distributed for free under free software for the General Public License. It has its basis on plane wave basis sets, density functional theory, and pseudopotentials both ultrasoft and norm-conserving. Quantum Espresso runs many calculations with powerful parallel machines, workstations and computer systems. These calculations involve ground state calculations, structural optimization, electrochemistry and special boundary conditions, response properties, spectroscopic properties and Quantum transport. The elastic constants indicate the deformation resistance along the axes and planes of the material under study. The band structure which represent the allowed electronic energy levels of solid materials, gives information on the material's electrical properties. It consists of the valence and conduction bands which overlaps. Between the conduction and valence bands the compound has superconducting gaps. The superconducting gaps are the energy differences between the valence band's highest points and the conduction band's lowest points. At external pressure application of 0.2GPa, the compound achieves phase transition and superconductivity emerges due to the reduction of the unit cell volume. The projected Density of states gives the number of states per energy range between the bands and shows the orbitals responsible for the conductivity. The phase change properties are brought about by changes in the conditions which induce desirable characteristics, for instance, superconductivity. Our results indicate that the compound is stable mechanically and with application of pressure it undergoes phase transition at 0.2GPa. From Density of states calculation, increase in energy results to phonon hardening a property which can be studies for its good application in integrated circuits.

LIST OF TABLES

LIST OF FIGURES

Page

LIST OF ABBREVIATION

ARPES   Angle Resolved Photoemission Spectroscopy

B   Bulk Modulus.

B_r Bulk – Reuss Approximation.

B_v Bulk – Voigt Approximation.

$CaFe_2As_2$.   Calcium Diiron Diarsenide

CHPC   Center for High Performance Computing

CT   Collapsed Tetragonal

DFT   Density Functional Theory

DFTB   Density Functional Tight Bind.

DOS   Density of States

DVM   Discrete Variation Method

E   Young Modulus.

ECP   Effective Core Potential

ESPRESSO   Open Source Package for Research in
                               Electronic, Structural Simulation and
                               Optimization.

E_{cut} Energy cutoff

FIG	Figure
FS	Fermi Surface
G	Shear Modulus.
GGA	Generalized Gradient Approximation
G_R	Shear – Reuss Approximation.
G_V	Shear – Voigt Approximation.
HF.	Hartree Fock Approximation
K	Wave vector.
K.E	Kinetic Energy.
LDA	Local Density Approximation
n	Poisson's ratio.
N_G	Number of Plane waves.
NMR	Nuclear Magnetic Resonance
NQR	Nuclear Quadrupole Resonance
PBE	Perdew Burke Enzerhof
PC	Point Contacts
PCAR	Point Contact Andreev Reflection

PDOS   Projected Density of states

P.E   Potential Energy.

PWscf   Plane wave self consistency field

RE   Rare Element

r_c Cutoff radius

SDW   Spin-Density Wave

TISE   Time Independent Schrodinger Equation

USPP   Ultrasoft Pseudopotential

V_{pp} Pseudopotential

2-D   2 dimension

CHAPTER ONE
INTRODUCTION

1.1 Background of Study

The iron pnictide compounds at stability form crystals at ambient pressure with a tetragonal shape at high temperatures. Phase change properties of these compounds are either triggered by the application of pressure or chemical doping. The iron pnictides with the extra hole per unit cell facilitate Na-doping to stabilize superconductivity. Na-substitution for Ca also induces superconductivity near 20K in polycrystalline material with nominal composition $Ca_5Na_5Fe_2As_2$ which, under pressure their resistivity lacks any sign of superconductivity in the first-order phase transition but has a reduction of its unit cell volume. Reduction of its unit cell volume and hole doping are essential for phase change properties. Electron doping suppresses structural phase transitions and superconductivity is induced. The Non-Magnetic Resonance and Nuclear Quadrupole Resonance measurements on the iron pnictides consistently found multiple gaps in phase change properties (Kohori, Yamato, Iwamoto, & Kohara, 2000).

$CaFe_2As_2$ has a tetragonal stable structure with one atom of calcium, two iron and two arsenide in the unit cell. At stability does not superconduct but upon excitation and doping it superconducts. Study of the compound's electronic, mechanical and structural transition properties is utilize its application on superconduction.

The appearances of several structural phases at low temperatures in $CaFe_2As_2$ are extremely sensitive to induced pressure (S. Saha et al., 2012). Also, by inducing internal strain, thermal treatment of the crystals at ambient pressure collapsed tetragonal phase is stabilized. Under hydrostatic pressure, the compound undergoes a structural transition to a phase of reduced c-axis length, which is collapsed tetragonal under low temperatures and registers no signature of

conductivity. Applied pressure overrun their phase change properties (Katayama et al., 2012). The high-temperature tetragonal state becomes orthorhombic and antiferromagnetically ordered as a function of pressure. At a pressure of 0.35GPa and low temperatures, transition takes place to a collapsed tetragonal state with a ~10% decrease.

Understanding phase transition properties of superconducting materials is important because of the wide range of applications (Huang, Fan, Singh, & Zheng, 2020). Magnetic levitation is where cargo vehicles, for instance trains can be suspended technically on very strong superconducting materials eliminating friction between trains and tracks. The superconductors will solve electrical energy wastage through heat and also utilizes space as they are smaller in size as compared to conventional electromagnets (Buongiorno et al., 2009).

Health practitioners require a non-invasive way of determining what is happening in human bodies. By impacting a strong superconductor-made magnet into the body, hydrogen and fat molecules in the body, except energy from a magnetic field, produce energy that can be identified and displayed graphically by the computer without carrying out surgery.

Superconductors are materials that do not resist the flow of current and are the most advanced in scientific discovery because they minimizes resistance (Scanlan, Malozemoff, & Larbalestier, 2004). Electric generators made with superconducting wires are more efficient and smaller as compared to conventional generators. These features enable them to be profitable ventures of power. They have energy storage that enhances power stability. Superconductor-based transformers are used in power utilities and fault limiters. Superconducting fault limiters have the ability to respond in very few seconds to limit huge amperes of current usage.

A weak link between two superconductors allows a small current to pass without energy dissipation (Silver & Zimmerman, 1967). On increasing current, it enables the junction to switch and does the output of single flux quantum whereby the switching is faster as compared to semiconductor transistors hence facilitating computing. It was identified in Mercury by Dutch physicist Heike Kemerling Onnes of Leiden University. He cooled the temperature of helium to 4K, and its resistance suddenly disappeared. An advancement came in 1962 when a graduate at Cambridge University predicted the flow of current in the two superconductors even when separated by a semiconductor (Josephson, 1993). This phenomenon is called Josephson Effect, applied to devices like squid that detect even the weakest magnetic field ever. Current iron pnictide superconductors have pushed transition temperature to 56K (Bartalesi, 2010) (Miyamoto et al., 2017) and they do not take the route of conventional superconductors. Operation of high Tc cuprates increased the tendency on pairing, raising superconducting transition temperature in terms of phonon coupling.

Superconductivity appears at a transition temperature $Tc=9.8K$ and $8.7K$ on doping group 10 elements such as Pd and Ni in $SrFe_2As_2$. In this material, resistivity exhibits metallic behavior and decreases below 17K, that is; resistivity is noticed at 15.6K(S. R. Saha, Butch, Kirshenbaum, & Paglione, 2010) (Meier, 2018), indicating superconducting transition at $T_c = 17K$. $SrFe_2As_2$ parent compound exhibits structural and long-range magnetic ordering phase transition at $T_o = 198 \, to \, 220K$ as a resistive anomaly. Resistivity exhibits no anomaly beyond T_c clearly shows that structural and magnetic ordering transition gets completely suppressed by *Platinum* substitution and superconductivity appears on the tetragonal phase in $SrFe_2As_2$ which is a contrast.

The iron pnictides have chemical packing that is not complicated and their structures do not differ so much in the alignment (Taylor 1971). They have a phase which ranges from paramagnetic to antiferromagnetic , transiting from tetragonal to orthorhombic. (Ran et al., 2011)

Change of the order parameter within different spin fluctuation sheets with multi gaps is responsible for superconductivity in the iron pnictides.

The Point Contact Andreev Reflection spectra have Point Contacts current in the Z-dependent *ab* plane on single crystals (Senkpiel et al., 2022), which greatly improves conductance in iron pnictides. First, it enhances conductance less than 20mV at around 10mV and secondly, below ~5mV-7mV. At around zero bias, conductivity is enhanced in the *ab* direction.

Iron pnictides are powerful magnets and when magnetism is removed through doping, superconductivity is enhanced. Superconductivity is facilitated in all iron-based superconductors by the application of pressure (Biswal & Mohanta, 2021). Iron pnictides possess superconducting symmetry and their pairing is out of spin fluctuations (Yin, Haule, & Kotliar, 2014).

Increases in the number of *Fe-d* bands close to the Fermi level by multiband effects enhance superconductivity. Forces of attraction and repulsion of multiband interactions improve superconductivity with both positive and negative band gaps.

The development of a coherent macroscopic quantum state of electrons facilitates superconductivity in metals. Superconducting transition temperatures of iron pnictides are high. When electrons move in unison conducting with no resistive loss of energy, we say superconductivity has been developed fully. Superconductivity rises as a result of an unconventional pairing mechanism between electrons due to coulomb interaction between electron-electron pairs called Cooper pairs which occurs at very low temperatures. Bad metal

properties at normal state and superconductivity occurring near antiferromagnetism order are the main features which facilitate superconductivity in *FeSCs* as opposed to conventional electron-phonon coupling and effectively, electron-electron pairs attractive forces are yielded as electrons avoid coulomb repulsion.

Quantum critical point appears at the border of the antiferromagnetism order (Hosoi et al., 2016), which affects the structure of the superconducting pairing greatly. *Fe* ions make a square lattice with *As* atoms below or above the center of the lattice (Chang et al., 2019). 111 iron pnictide group of materials comprise of three layers with *LaO* layers in between separating the layers. *F*-doping of the 111 iron pnictide family facilitates a transition temperature of 56K. In the 122 iron pnictide group for instance, $BaFe_2As_2$, each unit cell has two layers of *FeAs* with *Ba* ions in their midst separating them. Chemical substitution here gives rise to superconductivity with 38K maximum transition temperature attained.

$BaFe_2As_2$ is metallic, which develops antiferromagnetism order at Neel temperature (T_N) of 140K (Y. Wang, Lv, Zhu, & Ma, 2012). Iron based compounds above T_N are paramagnetic of which a good number are clear, enabling observation of quantum oscillations at low temperatures. They contain large sizes of electrical resistivity at room temperature an indication of bad metal. The bad metal properties indicate strong electron-electron correlation and put iron pnictides in the proximity of Mott localization.

This study is based on quantum mechanical theory under Density Functional Theory by considering the atomic simulation technique in the computation of the possible properties of the compound.

1.2 Statement of Research problem

Superconductivity has not been achieved in this compound by only pressure application as the only external condition. This study aims at the application of only pressure as the only physical condition and achieve structural phase transition with the emergence of superconductivity properties between external pressures of 0.1GPa and 0.3GPa. Superconductivity can be achieved upon conditions of temperature but our computational studies at CHPC works under room temperature and only pressure is varied.

Among the researched superconductors, a good number are type I superconductors. These are superconductors which lose superconductivity simply when placed in magnetic fields hence limiting their applications. $CaFe_2As_2$ compound is a type II superconductor whose superconductivity is not lost easily. They are known as hard superconductors and are applicable in many areas even in the strong magnetic fields.

1.3 Justification for the Study

Iron pnictides are essential in modern life in several ways, which necessitate research of their properties in the improvement of their wide range of applications. Superconducting wires made of iron pnictides are effective in the transmission of power as they have the least resistance. Electric generators made up of these wires are more efficient and smaller in size hence portable and manageable for the interest of space. They store energy and stabilize power supply. Superconductor-based transformers are used in power utilities and fault limiters, giving quick responses to avoid current wastage. In medicine determination of internal conditions of the body has been boasted by the use of superconductor-made magnets, which sends signals to the computers, making surgery unnecessary. Magnetic fields produce energy that can be identified and displayed graphically by the computer without carrying out surgery.

1.4 Objectives

1.41 Main Objectives

To apply *ab-initio* calculations in the study of the electronic, mechanical and phase change properties of iron pnictide compound $CaFe_2As_2$.

1.42 Specific Objectives

To investigate the effect of pressure **between 0.1GPa and 0.3GPa.**

    i.   On mechanical properties of $CaFe_2As_2$.

    ii.   On electronic structure properties of $CaFe_2As_2$.

    iii.   On phase change properties of $CaFe_2As_2$.

CHAPTER TWO
LITERATURE REVIEW

2.1 Introduction

This chapter gives a good summary of the literature review with a clear statement of the study gap and how this study intends to fill the gap.

2.2 Focus of Study

This research is focused on the computational simulation of materials with a specific interest in understanding mechanisms that control the chemical reactivity of nanostructured and nanoparticles in relationship to electronic structure properties. This field raises questions concerning the nature of bonding between molecules and atoms in regions of complex local environments and low symmetry. We shall bring understanding on how the bonding is affected by microscopic geometry, electronic structure, primary characteristics of molecules and atoms comprising various systems and atomic coordination. In view of this, we develop a framework for many-body modelling of materials whereby we bring to a comprehensive understanding at the atomic scale the properties of this material which provides physical insights and input parameters for further study (Richards et al., 2008). Material modeling studies have predictive powers which are considerable and are expected to provide the knowledge basis necessary for tailoring functional materials by design (Hufenbach et al., 2011). This fundamental comprehension of the chemical and physical characteristics at interfaces and surfaces forms the primary basis of computational research and development (Shi et al., 2015). The computational approaches, including molecular dynamics with density functional theory and empirical potentials for instance, describe the coupled transport of heat and matter in liquids and solids in a cost-effective manner (Caro & Victoria, 1989).

Experimentalists use computational experimentation in testing the effect of various parameters; since certain conditions are difficult to control in a laboratory. It is also noted that the experiment would be so expensive if it is to be done repetitively for many sets of parameters. For instance, Thomas Edison in inventing the first commercially viable electric light bulb, he tested thousands of materials to use for filament that would last long enough (David, 1991). This traditional process of trial and error of material discovery is the primary reason why we design very many materials by simulation more than 150 years later. Researchers can now avoid these many expensive dead ends, which slowed down Edison through a method known as materials by design. The material project launched in the year 2011, which is a Department of Energy program having a basis in Lawrence Berkeley national laboratory, plays a significant role in this evolution with a giant searchable repository of data available to the whole material science community. The use of computational material science that integrates quantum mechanics, supercomputers and advanced mathematics enables researchers to simulate thousands of compounds each day in search of the best candidates to give a test in the laboratory. They utilize a growing database of about 80,000 inorganic compounds in the selection of the existing materials and the creation of novel combinations for some given applications. Computational material science is far much efficient because material challenges underpin everything we do in science, engineering and technology. Computational work addresses questions on how to design materials that are stronger, lighter, cheaper to produce, less energy consuming and easier to make in the production process. Their applications have a very wide range of usage from battery material for the best next generation of cars to the replacement of the lead-based materials commonly used in gas stove lighters. In computational experimentations, scientists can explore both vertical and horizontal aspects in terms of properties interested in for specific materials.

There are countless and infinite numbers of combinations of atoms which can be computed until no more computational time is left. In order to accommodate a stream of material project calculations, scientists tap into a variety of supercomputing resources. Most of the material project work is about known materials, which give insights into the new materials. For instance, diamond is a material that is formed naturally at absolute pressures and temperatures deep down in the earth's mantle and is made use of in deriving parameters. Its qualities can be measured, for example, its hardness in association with its physical structure. From this beginning, it forms a basis for seeking other materials with similar structures which can be synthesized with a lot of ease. An example of a related material is silicon carbide, an important material used in braking systems due to its ability to withstand high temperatures. Silicon is much easier to make because it is just derived chemically not by physical parameters of pressure and temperature to create it.

Iron pnictides are iron-containing compounds and materials whose superconducting properties were revealed, which led to the discovery of iron pnictides, formerly known as oxypnictides. Later a sub-group of iron-based superconductors known as 122 iron arsenides with similar properties as the oxynitrides attracted attention because of their simple composition (Chiang, Dzyuba, Shevchenko, & Vasiliev, 2012).

2.3 Pnictides

These 122 iron pnictide compounds have a $ThCr_2Si_2$ structure with a space group of 14/mmm containing divalent alkali earth metal elements. It has been demonstrated in the recent past that trivalent *La* and monovalent *Na* can be combined, substituting the divalent ions successfully to form 122-type of superconductors with a 122-type of structure (Kawashima et al., 2018).

These compounds form crystals at ambient pressure with a tetragonal shape at high temperatures. Phase change properties of these compounds are either triggered by the application of pressure or chemical doping. The iron pnictides with the extra hole per unit cell facilitate *Na*-doping to stabilize superconductivity. *Na*-substitution for *Ca* also induces superconductivity near 20K in polycrystalline material with nominal composition $Ca_5Na_5Fe_2P_2$ which, under pressure, lacks any resistivity sign in the first-order phase transition but has a reduction of its unit cell volume. Reduction of its unit cell volumes and hole doping are essential for phase change properties. Electron doping suppresses structural phase transitions and induces superconductivity. 122 class of pnictide has an atomic arrangement of AFe_2As_2 with (A=Ba, Ca, Sr and Eu) atoms.

$CaFe_2As_2$ becomes a superconducting compound under pressure of 0.69 GPa, with a transition temperature T_c that exceeds 10 K (Chu & Lorenz, 2009). Single crystals of $CaFe_2As_2$ were synthesized and it was discovered that they possess first-order transition at a temperature of 170 K accompanied by structural and magnetic transition. Its superconductivity emerges upon chemical substitution (Sun et al., 2012). $CaFe_2As_2$ upon application of external pressure phase transition is suppressed by 0.35GPa and substituted by a first-order phase transition to a collapsed tetragonal that is magnetic at low temperatures. Further application of pressure to the compound marks the second transition with transition temperature crossing room temperature by 1.7 GPa (Canfield et al., 2009). In all these researches that have been done, superconductivity of $CaFe_2As_2$ has been achieved at relatively high pressures and temperature conditions which are expensive conditions to establish. Our research is geared towards achieving this important property in $CaFe_2As_2$ at relatively low and manageable pressure and at room temperature.

There is a serious need for magnetic resonance imaging techniques that require computer-generated radio waves and magnetic fields that will give well-detailed conditions of the body

tissues and organs to help diagnose the problem for specific and appropriate treatment. Electricity is used in the generation of these powerful magnetic fields but essentially requires superconducting wires of high magnetic tolerance.

New electricity generation, storage and delivery modes must be enhanced to meet the fast-growing global energy demand. Energy corporations will benefit from these innovations by using superconducting wires to avoid energy wastage and equally meet the high manufacturing costs. The metallic property of the iron pnictide compounds with less fragility allows molding them easily into long required wires in large quantities for devices like offshore wind turbines which grants an easy technology integration.

The modern improved superconducting generators have motors with minimized resistance to zero unlike the copper motors that have electrical resistance for enhanced efficiency. Superconducting generators provide reactive and faster power support, they are light and small in size hence portable with efficiency in power supply.

Superconductors have applications on cell phone base stations and powering coil guns, rail guns, improved fast digital circuits and particle detection. Superconductors are also required in instances of strong electric currents to protect equipment from melting. Superconductors also play an important role in allowing phones to operate with better reception and with very minimal power loss (Simon, Hammond, Berkowitz, & Willemsen, 2004).

CHAPTER THREE

THEORETICAL METHODS

3.1 Density Functional Theory

Density Functional theory is a quantum mechanical theory that takes consideration of the atomic simulation approach in the computation of a wide array of properties of all types of atomic systems that include; molecules, surfaces, crystals and electronic devices with their combination with non-equilibrium Green's functions. This theory has a basis in the electron density distribution as opposed to many-electron wave functions. It is used by both chemists and physicists in the conclusive calculation of the electronic structure of molecules, atoms and solids. Its applications had developed over time till in 1990 when its improvements were accepted in quantum chemical application after they were proved accurate, which resulted in an upsurge in applications. The Density Functional Theory is advantageous as it has a favorable performance ratio compared with other methods based on electron-correlated wave functions, coupled cluster and perturbation theory. This has led to the study of larger molecular systems with satisfactory accuracy hence enhancing the power to make predictions essential in electronic structure theory. The 1998 Nobel Prize that was awarded to Walter Kohn for his efforts in the development of the Density Functional Theory which is enough evidence that DFT is the most worldwide used electronic structure method of huge importance in physics and chemistry.

The molecular dynamics methods that have a basis on DFT for instance, the Born Oppenheimer and Car-Parrinello molecular dynamics have gained great fame in the recent past and are employed in many areas of physics, chemistry and bio molecular sciences. Classical molecular dynamics simulations that are fully based on less expensive force fields have been the areas of strength for bio molecular sciences. Variants based on DFT are more beneficial in studying

chemical reactions from First Principles as they have higher powers in making predictions than bespoke force fields. Molecular dynamics simulation based on DFT give room for reasonable characterization of chemical processes and molecular systems with a conclusive description of dynamical affinity at some given conditions of temperature. This has enhanced *ab initio* molecular dynamic investigations in more complex and larger condensed-phase molecular systems.

Hybrid methods have been developed to give descriptions of the central part of large systems by the use of quantum chemical methods, while classical molecular mechanics methods for instance, quantum mechanics provide a description of the surroundings. Quantum mechanical methods together with Density Functional theory are essential in the computation of physical parameters, which have direct links to the experiments. Theories and experiments team up and complement each other successfully not only in the obvious quantities but also in structures, energies and spectroscopic properties which are such crucial aspects of computation. Experimental spectra are interpreted by the electronic structure theory in many cases and are very necessary. Computational calculations of electron paramagnetic resonance and nuclear magnetic resonance using the First Principles and electron excitation in organic molecular systems is another study field greatly boosted by its important applications in photochemistry (Conti, Cerullo, Nenov, & Garavelli, 2020). The conventions advance on conventional Density Functional theory enabling calculations on the excited state properties beyond the recorded success of the conventional DFT in the analysis of the ground state properties. Currently, the popularity of the time-dependent density functional theory has improved the effective calculations of the excited states. Proper improvements on Born Oppenheimer approximation are

necessary to cater for the cases where the decoupling between electronic and nuclear motions does not hold.

These achievements have impacted much in the Density Functional theory in the study of biology, chemistry and physics. The effectiveness of the DFT has led to the treatment of more realistic systems allowing electronic structure theory to do more predictions which has expanded its potential for applications. This progress is so much improved by the continuous advancement in computer performance. Because of these tremendous achievements made, the joint computational and experimental results have been achieved more than 10 or 20 years ago.

Density Functional Theory focuses on electron density which is the number of electrons per unit cell volume on a specific point given by;

$$\rho(r) = \sum_i (\emptyset_i)(r)^2 \qquad\qquad 3.1$$

$\emptyset_i$ are the Kohn Sham orbitals of electrons which do not interact.

The total number of electrons is determined by the equation below;

$$\int \rho(r)dr = n \qquad\qquad 3.2$$

n is the total number of electrons.

A greater part of these studies is based on the DFT method, which has made it a more fashionable method of quantum mechanics presently. Thought provokingly approximate and uncomplicated versions of Density Functional theory for instance, the Density Functional Tight Bind (DFTB) method that is based on a second-order expansion of the DFT total energy have been developed simultaneously (Yang, Yu, York, Cui, & Elstner, 2007). By these empirical

methods that have a basis on DFT groundwork, the researcher has fast access to researching many systems in time scale and size in molecular dynamics simulations. The new advancement on the DFT directly benefits the Density Functional Tight Bind as it is built on the DFT.

Quantum states of a system of N electrons deal with 3N Cartesian coordinates in many body wave functions $\varphi(r_1 \ldots \ldots r_N)$ hence solving it is a challenge. The approximations that will be discussed later in the methodology simplify the equation and makes it easy to be worked upon (Zhang & Deng, 1993).

DFT enables us to link single wave functions with many body wave functions, get to know the equations satisfied by the wave functions and steps in the determination of the total energy of the system in the following manner.

$$E = <\varphi|H|\varphi> = \int d_{r1} \ldots \ldots \ldots d_{rN} \varphi^*(r_1 \ldots \ldots \ldots \ldots r_N) H^{\wedge} \varphi(r_1 \ldots \ldots \ldots \ldots r_m)$$

3.3

The Hamiltonian above is given by;

$$H^{\wedge}(r_1 \ldots \ldots \ldots \ldots r_N) = \sum_i \frac{\nabla_i^2}{2} + \sum_i V_n(r_i) + \frac{1}{2}\sum_{i \neq j} \frac{1}{|r_i - r_j|} \qquad 3.4$$

E is a functional of φ, $\quad E = F[n]$

A function takes an input function which returns a number as the output. The ground state energy which is the lowest possible energy of the system is a function of electron density only;

$$E = F(n)$$

$$n(r) \rightarrow E_e = F[n(r)] \qquad 3.5$$

$$\varphi(r_1 \ldots \ldots \ldots \ldots r_N) \rightarrow E \ E = F[\varphi(r_1 \ldots \ldots \ldots \ldots r_N)] \qquad 3.6$$

The Hohenberg-Kohn theorem state that the total energy of many-electron system is a functional of electron density (Kristyan, 2008). The following ways justifies this statement.

i. In the ground state, the external potential of nuclei v_n is determined uniquely by the electron density.

ii. The external potential v_n determines the many electron wave function in any quantum state; $v_n \rightarrow \varphi$.

iii. The total energy is a function of the many body wave functions in any quantum state.

iv. In keen and close consideration of the justifications, we conclude that in the ground state the total energy is determined by the density.

$$n \rightarrow v_n \rightarrow \varphi \rightarrow E$$

$$E = F[n]$$

$$\text{T} = -\sum_i \frac{1}{2}\nabla_i^2 \text{W} = \frac{1}{2}\sum_{i \neq j} \frac{1}{r_i - r_j \vee} \qquad 3.7$$

Hence total energy is:

$$E = \langle \varphi \sum_I V_n(r_i) \vee \varphi \rangle + \langle \varphi \vee \text{T} + \text{W} \vee \varphi \rangle \qquad 3.8$$

The solution to the following Kohn Sham equations will help us in the calculation of the total energy with a lot of ease;

$$\left[-\frac{1}{2}\nabla^2 + V_{tot}(r) \right] \emptyset_i(r) = \varepsilon_i \emptyset_i(r) \qquad 3.9$$

$$V_{tot}(r) = V_n(r) + V_H(r) + V_{Xc}(r) \qquad 3.10$$

$$V_n(r) = -\sum_I \frac{Z_I}{|r - R_I|} \qquad 3.11$$

$$\nabla^2 V_H(r) = -4\pi n(r) \qquad\qquad 3.12$$

$$V_{Xc}(r) = \frac{\delta E_{xc}[n]}{\delta n}(r) \qquad\qquad 3.13$$

$$n(r) = \sum_i |\emptyset_i(r)|^2 \qquad\qquad 3.14$$

Equation 3.9 is the standard single particle Schrödinger equation which is solved as a single eigenvalue problem. To determine eigenvalues ε_i and the eigen functions $\emptyset_i$, there is a need to first know the sum total potential $V_{tot}(r) = V_n(r) + V_H(r) + V_{Xc}(r)$. The only challenge at this level is that $V_{Xc}(r)$ and $V_H(r)$ depends on the electron density n and the electron density depends on the unknown eigen functions $\emptyset_i$ through eqn 3.14. This means that each solution $\emptyset_i$ is dependent entirely on all other solutions $\emptyset_i$ hence linked with each other in eqn 3.9- eqn 3.14 which implies that all must be solved self-consistently.

Self-consistency in this case means, if we insert $\emptyset_i$ solution in the $n(r) = \sum_i |\emptyset_i(r)|^2$ equation and calculate the density, determine the corresponding potential V_{tot} by $V_{tot}(r) = V_n(r) + V_H(r) + V_{Xc}(r)$ and proceed in the calculation of the Schrödinger Equation, then we get a solution $\emptyset_i$ which we had begun with at that point we would have achieved self-consistency.

The practical procedure to find the solution of the Kohn Sham equations, eqn 3.9- eqn 3.14 is by specifying the nuclear coordinates in the calculation of the nuclear potential $V_n(r)$ beginning with eqn 3.11. Essentially this information is made available in the crystallography data.

In particular, the beginning point is by trying to give solution to eqn 3.9 by the use of $V_n(r)$ as the first approximation which is more convenient in giving a 'guess' of the possible electron density $n(r)$ for the determination of the preliminary approximation of the Hartree exchange

correlation potentials. We will make our initial guess for the electron density by the summation of the densities that correspond to totally isolated atoms but maintaining the arrangement of the atomic positions as per the material under study.

We make use of the density in obtaining the initial estimates of the Hartree exchange correlation potentials $V_H + V_{Xc}$ and then V_{tot}.

We proceed in the solution of the numerical Kohn-Sham equations (Aichinger & Krotscheck, 2005). Solving Kohn-Sham equations gives rise to new wave functions which in turn, we make use of in the construction of new estimates of the total potential and density n. This procedure is repeated to a point where the new density matches with the old density within some given desired tolerance, the point where self-consistency is achieved. The process is illustrated as shown below:

Schematic flow chart that is used to find self-consistent solutions for the Kohn-Sham equations.

Construct initial density

$\rho_{old}(r)$

$\rho_{old}(r)\rho_{new}(r)$

Construct new density $\rho_{new}(r)$ with $\rho_{old}(r)$ and previous

Construct effective potential $V_{eff}(r)$ with old density

$\rho_{old}(r)$

Solve Kohn Sham equations

$$\left[\frac{-1}{2}\nabla^2 V_{eff}(r)\right]\varphi^v_{k(r)} = \varphi^v_{k(r)}$$

Calculate electron density $\rho_{old}(r)$ solves the given problem

Construct ground state density

Test Convergence of density $|\rho_{old}(r) - \rho_{old}(r)|V_{\rho_{conv}}$

Calculate electron density $\rho_{old}(r)$ solves a given problem

3.2 Methodology

This part contains a description of the different methods adopted in the quest to address the research question and in the achievement of the research objectives. This study makes use of QUANTUM ESPRESSO, which is an integrated suite of the open source computer coding used for quantum simulation of material projects by the use of state-of-the-art electronic structure approaches which have a strong basis on density functional theory, many-body perturbation theories and density functional perturbation theory (Marini, Poncé, & Gonze, 2015) under projector augmented wave and plane wave pseudo potential techniques (Kresse & Joubert, 1999). QUANTUM ESPRESSO has grown its popularity in the processes and it is possible to study a wide variety of properties of materials through simulation (Giannozzi et al., 2017). The high performance of QUANTUM ESPRESSO is on an increasingly emerging broad package of hardware architectures and a great community of research which relies on its abilities of the fundamental open source platform development and implementation of the upcoming ideas. Numerical simulations of density functional theory have become popular and powerful tool used in studying material properties . Many such simulations are based on plane wave pseudopotential methods that use the projector augmented wave method (PAW) or often use Ultra soft pseudo potential . QUANTUM ESPRESSO is highly anchored on modularity, openness, innovation and efficiency   (Hussain, Shah *et al*; 2022). Its distribution is based on two important effective packages, *CP* and *PWscf* which perform molecular dynamics calculations and self-consistent calculations respectively *(*Goldsmith, Andrade *et al*; 2021) plus the other many additional packages that are used in the more advanced calculations (Ganose, Jackson *et al*; 2018, Hung, Nugraha *et al*. 2022) including; *Phonon*, *PostProc*. *Atomi*c, *XSpectra*, *GiPAW*, *turboTDDFT*, *turboEELS*, *QE-GiPAW*, *GiPAW*, *EPW*, *Sternheimer GW*, *GWL*, *Thermo_PW* , *Thermal2, d3q*.

3.3 Calculation Procedure

The experiments began with self-consistent field calculations, which involved the selection of approximate Hamiltonian that led to the solution of the Schrödinger equation in obtaining a more accurate set of orbitals and repeated the solution of the Schrödinger equation with the obtained new orbitals until the results converged. This determined energy of its many-body system in the stationary state and centrally aimed at identifying the lowest energy arrangement of the individual atoms. We performed non-self-consistent field calculations immediately after self-consistent, which enabled the sampling of the system to a denser space allowing subsequent calculations such as crystal structure, mechanical properties, band structure, density of states and projected density of states. This research was based on the application of external pressure in determining properties that include elastic constants calculation which gave the measure of the proportionality between stress and strain in the crystal brought about by the application of pressure. The performed density of states and projected density of states calculations described the number of modes for each single frequency range and computed information about the different contributions of the different orbitals, respectively.

The first principle calculation study of $CaFe_2As_2$ under induced pressure was undertaken in the framework of density functional theory (DFT) based on plane wave self-consistent field (PWscf) and ultra-*soft pseudopotential* (USPP) method as treated in the Perdew-Burke Ernzerhof (PBE) (Idrissi, Labrim *et al*; 2021) generalized gradient approximation and local density approximation. The computational calculations were performed using Quantum Espresso simulation package and the optimized cell dimensions were fitted using Murnaghan fitting methodology (Jin et al., 2022) given as;

$$P = 1.5B_o \left[\frac{V^{\frac{7}{3}}}{V} - \left(\frac{V_o}{V}\right)^{\frac{5}{3}} \right] \left[1 + 0.75(B_o' - 4) \left(\left\{\frac{V_o}{V}\right\}^{\frac{2}{3}} - 1 \right) \right]$$ 3.15

B_o-*Initial Bulk modulus*

B_o'- *delivative of bulk modulus*

V_o-*initial volume*

v-*final volume*

The *k* points, and the kinetic energy cut-off values were properly checked through graphing and accurate values were obtained for the convergence of the ground state energy at minimum convergence threshold in the calculation using the proper basis sets (Halkier et al., 1998). The minimization is given by the relation in eqn. 3.16;

$$E(V) = E_o + \frac{9V_oB_o}{16} \left\{ \left[\left(\frac{V_o}{V}\right)^{\frac{2}{3}} - 1 \right]^3 B_o' + \left[\left(\frac{V_o}{V}\right)^{\frac{2}{3}} - 1 \right]^2 \left[6 - 4\left(\frac{V_o}{V}\right)^{\frac{2}{3}} \right] \right\}$$ 3.16

E_o- *initial energy*

E_o, B_o' and B_o are the minimum energy, the derivative of bulk modulus and the bulk modulus for pressure.

The optimization was achieved by considering the volume at minimum energy in the pressure-volume graph and energy-volume graph using the Birch Murnaghan equation fitting of second order (Levämäki, Tian, Vitos, & Ropo, 2019). The valence configuration used for $CaFe_2As_2$ was $3s^23p^64s^2$ for Ca, $3s^24s^23p^6$ for Fe and $4s^24p^3$ for As. The convergence threshold was estimated at 10^{-8} eV which is sound for accuracy. The Brillouin sampling was based on the Monkhost

scheme (da Jornada, Qiu, & Louie, 2017). The K-point mesh of the irreducible high symmetry points in the Brillouin zone used was 6 x 6 x 4. For the elastic constant calculation, the 'quasi-static' approximation was used, where the elastic constants were computed at absolute temperature and saved as elastic constants.

3.31 Mechanical Properties Calculation

Mechanical properties play significant role in the crystal structure studies. Empirically, mechanical properties of materials are determined by elastic properties which include the shear modulus (G), bulk modulus (B), Young modulus (E), and Poisson's ratio (*n*).

Specifically, elastic properties are achieved by the elastic constants (C_{ij}), which are identified as the stress tensor versus small strain. Additionally, the mechanical stability of materials is calculated by elastic constants. For cubic crystal structure, there exist three independent elastic constants; $C_{11,}$ C_{12}, and C_{44}, which determine the mechanical stability given by Borh's stability criteria;

$$C_{11} > 0, C_{44} > 0, C_{11} > C_{12} \; C_{11} + C_{12} > 0 \qquad\qquad 3.17$$

In a tetragonal stable crystal structure, there are six elastic constants; C_{11}, C_{12}, $C_{13,}$ C_{33}, C_{44}, and C_{66}. Mechanical stability of this structure is evaluated by;

$$C_{11} > 0, \; C_{33} > 0, \; C_{44} > 0, \; C_{66} > 0,$$

$$C_{11} - C_{12} > 0, \; C_{11} + C_{33} - 2C_{13} > 0,$$

$$2(C_{11} + C_{12}) + C_{33} + 4C_{13} > 0. \qquad\qquad 3.18$$

State of mechanical stability for tetragonal structure can be well evaluated by Borh-Huang criteria (Voigt 1928) in eqn. 3.18;

$C_{ii} > 0$ (i=1, 3, 4, 6)

$C_{11} + C_{33} - 2C_{13} > 0$

$2(C_{11}+C_{12}) + C_{33} + 4C_{13} > 0$ 3.19

$C_{11} - C_{12} > 0$

Taking into account the structural symmetry, the shear and bulk moduli are evaluated in compliance with Voigt-Reuss-Hill (VRH) approximation. Additionally, Young's modulus is identified to be the ratio of linear strain versus linear stress, which gives the degree of elastic stiffness. Poisson's ratio indicates the advances of the covalent bond. A high ratio proves the presence of ionic and metallic bonds. Values of C_{ij} can be used in the evaluation of Poisson's ratio and elastic moduli of $CaFe_2As_2$. As per Voigt approximation, the bulk modulus together with the shear modulus isotropy can be acquired by doing linear combination of elastic constants (Panda & Chandran, 2006). With a different format, Reuss obtained estimates for bulk modulus and shear modulus isotropy by employing the use of elastic constants for a single crystal (Panda & Chandran, 2006). Hill confirmed that Voigt and Reuss estimates were lower and upper polycrystalline elastic moduli limits respectively, hence the averages became realistic as shown in Eqn. 3.20.

$$B = \frac{B_V + B_R}{2}$$

$$G = \frac{G_V + G_R}{2}$$ 3.20

$$B_V - bulk - voigt\ modulus$$

$$B_r - bulk\ reuss\ modulus$$

The elastic anisotropy of a material's crystal is the material's orientation dependent on the elastic moduli (Sakurada, Nukushina, & Ito, 1962). A well description of the crystal's elastic anisotropy plays an important role in solid state physics as well as the engineering science area. The term anisotropy is used in the description of the direct dependent properties of materials. For instance magnetic anisotropy which may occur in plasma which enables the magnetic field oriented in a desired direction (Schekochihin, Cowley *et al*; 2005). Directional filamentation is shown by plasmas in lighting and plasma globe. Many materials are optically anisotropic which the anisotropy of light is. To determine the quantity of the elastic anisotropy of the material in the tetragonal structure, there is need to evaluate the Zener anisotropic factor given by $A = 2 \, C_{44}/(C_{11} - C_{12})$ (Dragomir & Ungár, 2002).

For the completely isotropic materials *A=1* while for the anisotropic material value of *A* is either smaller or greater than one. Another parameter for anisotropy for tetragonal materials is given by the ratio between coefficients of linear compressibility along the *a* and *c* axis K_c/K_a (Bridgman, 1964). For isotropic crystals the compressibility on both directions is the same and the value is a unit while a less or greater value the unit indicates that compressibility along *a* axis is either larger or smaller than *c* axis.

In determining whether the material is isotropic, the relationship below was used;

$$A^U = \frac{5G_V}{G_R} + \frac{B_V}{B_R} - 6 \qquad\qquad 3.21$$

Whereby if A^U=0 the material would be regarded as isotropic. As shall be shown, our calculations indicate that the material is anisotropic with a value of 0.1807, which is in agreement with the studies of the parent compound $ThCr_2Si_2$ (Siggelkow, Hlukhyy, & Fässler, 2010).

Pressure, which is the main basis for phase transition, was calculated for a good range of volume by the relationship eqn. 3.22;

$$H(P) = U(V[P]) + PV \qquad\qquad 3.22$$

Structural transition is associated with the atomic packing and orientation in the crystal, which brings about the change of the related properties of the compound. This change is due to different conditions, for instance, temperature and pressure. Given that our calculations are done at ground state temperature, only the pressure is varied in these calculations.

Superconductivity of this material which is the main focus of this study appears at structural phase transition point brought about by the application of external pressure. Optimization of the cut-off energy convergence was achieved at 45 Ry with k-point mesh of 6x6x4.

There exist three axes in the tetragonal crystalline structure with a different length of the central axis either shorter or longer than the other two (Mazzi, Galli, & Gottardi, 1976). The remaining two axes have the same lengths and lies in the same plane. A material with a tetragonal system has a body centered tetragonal cells and their Bravais lattice is given in such a way that a and b are equal but not equal to c and α, β and γ are all equal to 90 degrees.

3.32 Many-body Schrödinger Equation

In the effort of understanding the behavior of quantum particles there is an essence to determine the corresponding wave function $\varphi(r)$ for each point $r = xU_x + yU_y + zU_z$ in a point of interest by solving Schrödinger equation. xU_x, yU_y, zU_z denotes unit vectors along the Cartesian axes. The emphasis is restricted to the stationery states by considering time independent Schrödinger equation which has the following form;

$$(K.E + P.E)\varphi = E\varphi \qquad\qquad 3.23$$

E is the eigenvalue energy described by the wave function φ for stationery states. The probability to find a particle at point r is $|\varphi(r)|^2$. An electron in a potential energy landscape $v(r)$ eqn 3.23 is written explicitly as;

$$\left[\frac{p^2}{2me} + V(r)\right]\varphi(r) = E\varphi \qquad\qquad 3.24$$

m_e is the electron mass and p is the quantum mechanical momentum operator which is given as;

$$p = -i\hbar\nabla, \nabla = \frac{\partial}{\partial_x}i^\wedge + \frac{\partial}{\partial_y}j^\wedge + \frac{\partial}{\partial_z}z^\wedge \qquad\qquad 3.25$$

$\hbar$ is the reduced Planck constant.

φ_0 is the lowest energy solution of eqn 3.24. For a system at equilibrium, the electron occupies the lowest energy configuration φ_0. At equilibrium, the electron charge density is given by $|\varphi(r)|^2$. If one electron is added to the system, in the determination of the new distribution of electronic charge by the use of Pauli Exclusion Principle, the new electron is accommodated in the same eigenstate φ_0 as long as the two electrons have opposite spins. By adding $|\varphi_0|^2$ the electronic charge distribution becomes $2|\varphi_0|^2$. The two electrons tends to repel each other and in the repulsive interaction modifies both the potential term V and φ_0 , and shape in eqn 3.24. A proper description of systems with many electrons and nuclei need to be considered which modifies eqn 3.25. Here many body wave function Ψ is introduced which is dependent on electrons and nucleus position in the system. For N electrons of coordinates $r_1, r_2, \ldots\ldots r_N$ and M nuclei of coordinates $R_1, R_2, \ldots\ldots R_M$ we have;

$$\Psi = \Psi(r_1, r_2, \ldots\ldots r_N; R_1, R_2, \ldots\ldots R_M) \qquad\qquad 3.26$$

$|\Psi = \Psi(r_1, r_2, \ldots \ldots r_N; R_1, R_2, \ldots \ldots R_M)|^2$ is the new probability to find an electron 1 at point r_1, electron 2 at point r_2 and so on. Here our interest is on electronic charge density defined as the probability to find an electron at position r. $p(r_1 = r)$ probability of finding electron 1 at r when others could be anywhere basically is the logical 'OR' combination of all the configurations whereby $r_1 = r$ and $r_2, \ldots \ldots r_N$, spans the entire volume of the material.

$$p(r_1 = r) = \int \Psi(r_1, r_2, \ldots \ldots r_N; R_1, R_2, \ldots \ldots R_M)|^2 \, dr_2, \ldots \ldots dr_N \, dR_1, \ldots \ldots dR_M \quad 3.27$$

The electron density is then given as;

$$`n(r) = p(r_1 = r) + p(r_2 = r) + \ldots \ldots \ldots + p(r_N = r) \quad 3.28$$

Because in quantum mechanics electrons are the indistinguishable particles whereby each term of the right hand side of eqn 3.28 is given by eqn 3.27 hence eqn 3.28 is written as;

$$n(r) = N \int \Psi(r_1, r_2, \ldots \ldots r_N; R_1, R_2, \ldots \ldots R_M)|^2 \, dr_2, \ldots \ldots dr_N \, dR_1, \ldots \ldots dR_M \quad 3.29$$

If the many body wave function Ψ is normalized to a unit within a material;

$$\int \Psi(r_1, r_2, \ldots \ldots r_N; R_1, R_2, \ldots \ldots R_M)|^2 \, dr_2, \ldots \ldots dr_N \, dR_1, \ldots \ldots dR_M = 1 \quad 3.30$$

Combining eqn 3.30 with eqn 3.29, the integral of the electronic charge density of a material throughout the entire material gives the number of electrons N;

$$\int n(r) dr = N \quad 3.31$$

For the introduction of the many body wave function eqn 3.24 becomes;

$$(K.E + P.E)\Psi = E_{tot}\Psi \quad 3.32$$

E_{tot} eigenvalue is now representing the total energy of the system.

Taking into account N electrons and M nuclei , the Kinetic energy in eqn 3.32 is given as;

$$K.E = -\sum_{I=1}^{N} \frac{\hbar^2}{2m_e} \nabla_I^2 - \sum_{I=1}^{M} \frac{\hbar^2}{2M_I} \nabla_I^2 \qquad 3.33$$

$M_1, M_2, \ldots..$ are the masses of nuclei.

Laplace operator ∇^2 derivatives are taken with respect to the coordinates of every particle for instance;

$$\nabla_I^2 \Psi = \frac{\partial^2 \Psi}{\partial x_1^2} + \frac{\partial^2 \Psi}{\partial y_1^2} + \frac{\partial^2 \Psi}{\partial z_1^2} \qquad 3.34$$

For potential energy we simplify the equations by counting the possible pairs of charges in the system.

1st Coulomb repulsion between electron pairs

$$(P.E)_{ee} = \frac{1}{2} \sum_{i \neq j} \frac{e^2}{4\pi\epsilon_0} \frac{1}{|r_i - r_j|} \qquad 3.35$$

i and j run from 1 to N. $i \neq j$ is excluded because an electron does not repel itself but repels another electron at another position. It is divided by 2 in order to count only one contribution per pair.

2nd Coulomb repulsion between pairs of nuclei

$$(P.E)_{nn} = \frac{1}{2} \sum_{I \neq J} \frac{e^2}{4\pi\epsilon_0} \frac{Z_I Z_J}{|R_I - R_J|} \qquad 3.36$$

Atomic number is represented by Z and indices I and J run from 1 to M and the 3rd Coulomb attraction between electrons and nuclei

$$(P.E)_{en} = -\sum_{iI} \frac{e^2}{4\pi\epsilon_0} \frac{Z_I}{|r_i - R_I|}$$ 3.37

I from 1 to M and j from 1 to N.

Combining eqn 3.32 to eqn 3.37, the many body Schrodinger equation becomes;

$$\left[-\sum_i \frac{\hbar^2}{2M_e} \nabla_i^2 - \sum_I \frac{\hbar^2}{2M_I} \nabla_I^2 + \frac{1}{2}\sum_{i\neq j} \frac{e^2}{4\pi\epsilon_0} \frac{1}{|r_i - r_j|} + \frac{1}{2}\sum_{I\neq J} \frac{e^2}{4\pi\epsilon_0} \frac{Z_I Z_J}{|R_I - R_J|} - \sum_{iI} \frac{e^2}{4\pi\epsilon_0} \frac{Z_I}{|r_i - R_I|} \right] \Psi = E_{tot}\Psi$$

3.38

Equation 3.38 is everything we need in studying behavior of materials at equilibrium. Solving eqn 3.38 and finding the eigenstates with lowest energy known as the ground state energy of a system, a good number of the equilibrium properties of materials can be calculated from elastic properties up to enthalpies of formation, phase diagrams and thermal properties. The challenge is that the solution of eqn 3.38 for all simplest systems for instance very small molecules is practically impossible. For example the description of the nuclei and electrons in the unit cell of a crystal like silicon, the volume of the unit cell of a diamond structure is $a^3/4$ with $a = 5.43\text{Å}$.

A possible discretization of the unit cell volume would have points spaced by $\Delta x \sim 0.1\text{Å}$. such grid could consist $N_p = a^3/4/(\Delta x)^3 \sim 40,000$. To count four valence electrons for each of the atoms of silicon in a single unit cell as the well as the nuclei $N + M = 10$ particles, the specifications of the quantum state will require $N_P^{N+M} \sim 10^{46}$ complex numbers. To perform matrix operations with arrays of these complex numbers is obviously impossible. The complexity of the equation increases with the increase in size of the system. As a result, we have hierarchy of approximations to eqn 3.38 which enables study of materials at atomistic level with varying degrees of accuracy and complications.

3.321 Atomic Units

The eqn 3.39 above is simplified to give the likelihood of finding its solution. Before simplifying it further, it is convenient to do the housekeeping of the units of measurements. The quantities that are required to be determined from experiments are the electron density, *me*, reduced Planck constant $\hbar$, the electron charge, e, permittivity of vacuum, ϵ_0, and the nuclear masses, M_I, for naturally occurring elements, their nuclear masses are known and ranges.

We assume the following;

$$\hbar = 1.05457163.10^{-34} J.S$$

$$m_e = 9.10938291.10^{-31} Kg$$

$$m_p = 1.67262164.10^{-19} C$$

$$\epsilon_0 = 8.8541878210^{-12} F/m$$

The quantities given above are fundamental physical constants which do not depend on any given particular material under study. Eqn 3.38 has no empirical parameters which would require to be obtained for instance from estimates, measurements or data fitting procedures, this study of material properties is referred to as 'First Principles Approach '.

3.322 Clamped Nuclei Approximation

After specifying atomic units and the fundamental physical constants, there is need to sort the mechanisms that will give a solution to the equation 3.39. At this point, the equation is describing generally everything in the states of matter hence not specific. In liquids and gases, the inter-molecular distances are considerably large therefore and the intermolecular forces are weak making the nuclei to travel long distances. Emphasis is put on solids and molecules where the nuclei remain typically in certain known positions and we make the assumption that nuclei are held clamped (immobile) in known positions. Here we concentrate on electrons which are

mobile as the nucleus is in a fixed position. For the nuclei to be immobile, it means that the nuclei are so heavy hence their nuclear masses are set to infinity $M\infty$. This indicates that we neglect the kinetic energy of the nuclei and the coulomb repulsion between nuclei becomes a constant (Nolen Jr & Schiffer, 1969). The is reduced to;

$$\left[-\sum_i \frac{1}{2}\nabla_i^2 - \sum_i V_n(r_i) + \frac{1}{2}\sum_{i\neq j}\frac{1}{|r_i-r_j|}\right]\Psi = E_{tot}\Psi \qquad 3.39$$

We give a definition of the coulomb potential of the nuclei by regarding φ as a function of electron coordinates and nuclear coordinates R_I as external parameters (Liu & Liang, 2011).

$$V_n(r) = -\sum_I \frac{ZI}{|r-R_I|} \qquad 3.40$$

Defining many electron Hamiltonian;

$$H^\wedge(r_1, r_2, \ldots r_N) = -\sum_i \frac{1}{2}\nabla_i^2 \pm \sum_i V_n(r) + \frac{1}{2}\sum_{i\neq j}\frac{1}{r_i-r_j\vee} \qquad 3.41$$

$$H\Psi = E\Psi \qquad 3.42$$

Single electron Hamiltonian becomes;

$$H_0(r) = \frac{-1}{2}\nabla^2 + V_n(r) \qquad 3.43$$

$$\mathrm{H}(r_1, r_2, \ldots r_N) = \sum_i \mathrm{H}_0(r_i) + \frac{1}{2}\sum_{i\neq j}\frac{1}{|r_i-r_j|} \qquad 3.42$$

3.323 Independent Electrons Approximation

From the equation 3.42 above the only interaction term remaining is the term describing Coulomb repulsion between electrons hence solving it will give some light to the solution of the

equation. Removal of this term will imply that the electrons don't 'see' each other therefore no interaction between electrons which contributes to the total energy.

$$\sum_i \hat{H_0}(r_i)\Psi = E\Psi \qquad 3.43$$

The electrons become independent hence the probability $|\varphi_0(r_1, r_2, \ldots r_N)|^2$ of the first electron at r_1, second electron at r_2 and electron N at r_N is given by the product of individual probabilities $|\varphi_0(r_i)|^2$ of finding ith electron at N (Shemansky & Broadfoot, 1971).

$$\varphi(r_2, \ldots r_N) = \emptyset_1(r_1) \ldots \ldots \emptyset_N(r_N) \qquad 3.44$$

The wave function $\emptyset_i$ is obtained as solutions for single electron Schrödinger equation.

$$\hat{H_0}(r)\emptyset_i(r) = \varepsilon_i\emptyset_i(r) \qquad 3.45$$

$$\left[\sum_i \hat{H_0}(r_i)\right]\emptyset_1(r_1) \ldots \ldots \emptyset_N(r_N) = E\emptyset_1(r_1) \ldots \ldots \emptyset_N(r_N) \qquad 3.47$$

This equation is single electron Hamiltonian hence $\hat{H_0}(r_1)$ acts only on $\emptyset_i(r_1)$. $\hat{H_0}(r_2)$ acts on $\emptyset_2(r_2)$ and so on. Therefore, we can rewrite the equation as;

$$\left[\hat{H_0}(r_1)\emptyset_i(r_1)\right]\emptyset_2(r_2) \ldots \ldots \emptyset_N(r_N) + \emptyset_i(r_1)\left[\hat{H_0}(r_2)\emptyset_2(r_2)\right] \ldots \ldots \emptyset_N(r_N) + \cdots \ldots$$
$$= E\Psi_1(r_1) \ldots \ldots \Psi_N(r_N)$$

Using equation 3.45 we have;

$$E = \varepsilon_1 + \varepsilon_2 + \ldots \ldots + \varepsilon_N \qquad 3.47$$

3.324 Exclusion Principle

This principle states that electrons are 'fermions' hence the many-body wave function Ψ must change sign when the variables of two electrons are exchanged. The exchange involves the positions and the spin of electrons. The principle simply states that no two electrons can occupy the same electronic state. Electrons of the wave functions $\emptyset_1(r_1)\emptyset_2(r_2)$ with $\emptyset_1 \neq \emptyset_2$ does not satisfy the requirement but the wave functions does (Kutzelnigg, Del Re, & Berthier, 1968).

$$\Psi(r_1, r_2) = \frac{1}{\sqrt{2}}[\emptyset_1(r_1)\emptyset_2(r_2) - \emptyset_1(r_2)\emptyset_2(r_1)]^2 \qquad 3.48$$

Writing the equation in a matrix determinant called Slater determinant.

$$\Psi(r_1, r_2) = \frac{1}{\sqrt{2}}\begin{vmatrix} \emptyset_1(r_1)\emptyset_1(r_2) \\ \emptyset_2(r_1)\emptyset_2(r_2) \end{vmatrix} \qquad 3.49$$

Electron charge density of independent electrons is the total sum of the probabilities of finding electrons in each of the occupied state i.

$$n(r) = \sum_i |\emptyset_1(r)|^2 \qquad 3.50$$

3.325 Mean Field Approximation

Distribution of electronic charge $n(r)$ generates potential $\varphi(r)$ by Poisson's equation (Aichhorn, Pourovskii *et al*; 2009).

$$\nabla^2\varphi(r) = 4\pi n(r) \qquad 3.51$$

Electrons in electrostatic potential contain Hartree potential which satisfies Poisson's equation.

$$V_H(r) = -\varphi(r)$$

$$\nabla^2 \varphi(r) = -4\pi n(r)$$

$$V_H(r) = \int dr' \frac{n(r')}{|r - r'|}$$

$$\left[\frac{\nabla^2}{2} + V_n(r) + V_H(r)\right]\emptyset_i(r) = \epsilon_i \emptyset_i(r)$$

$$n(r) - \sum_i |\emptyset_i(r)|^2$$

$$\nabla^2 V_H(r) = 4\pi n(r) \qquad\qquad 3.52$$

3.326 Hartree-Fock Equations

When electrons are not interacting with each other it means many body wave function is written as a Slater determinant to obtain single particle wave function as a solution to single particle Schrödinger Equation. Single wave functions are found by the use of variational principle. A quantum state of the lowest energy is found by multiplying both sides by φ and doing integration (Chetyrkin & Tkachov, 1981).

$$E = \int dr_1 \ldots\ldots\ldots dN \varphi^* \hat{H} \varphi \qquad\qquad 3.53$$

$$E = \langle \varphi^* \hat{H} \varphi \rangle \qquad\qquad 3.54$$

Minimizing E with respect to $\emptyset_i(r)$ in the slater determinant the functions need to be orthonormal.

$$\frac{\delta E}{\delta \emptyset_i^*} = 0$$

$$\int dr\, \varphi^*(r)\emptyset_j(r) = \delta_{ij} \qquad\qquad 3.55$$

δ_{ij} −Kronecker delta and is equal to 1 if $i = j$ and 0 if $i \neq j$. Then we find the Hartree-Fock equations (Lions 1987).

$$\left[\frac{-\nabla^2}{2} + V_n(r) + V_H(r)\right]\emptyset_i(r) + \int dr' V_x(r,r')\emptyset_i(r) = \epsilon_i\emptyset_i(r)$$

$$n(r) - \sum_i |\emptyset_i(r)|^2$$

$$\nabla^2 V_H(r) = -4\pi n(r)$$

These equations have an additional potential V_X

$$V_X(r,r') = -\sum_i \frac{\emptyset_j^*(r')\emptyset_j(r)}{|r-r'|} \hspace{3cm} 3.56$$

An advantage of these equations is that they move us from classical electrons to quantum electrons. On the other hand it is disadvantageous as they introduces a non-local potential $V_X(r,r')$ whose integration complicates the practical solution.

3.327 Kohn-Sham Equations

Here equation is simplified by eliminating Coulomb interaction of the electrons and the transformed *3N*-dimensional many body Schrödinger equations into N three-dimensional equations. So far the correlation between electrons term is the only term remaining to be simplified. As to Coulomb repulsion the probability to find an electron decreases if there exists another electron near as shown in eqn 3.57 (Harrison, 1985).

$$|\varphi_0(r)|^2 + |\varphi_0(r)|^2 = 2|\varphi_0(r)|^2 \hspace{3cm} 3.57$$

Repulsion is defined by an additional component $V_i(r)$ for correlation. Also replace the complicated exchange potential with a simpler version with same effect but depends on only one space coordinate $V_x(r)$ which is the simplified local exchange potential (Hedin & Lundqvist, 1971).

$$\left[\frac{-1}{2}\nabla^2 + V_n(r) + V_H(r) + V_X(r) + V_C(r)\right]\emptyset_i(r) = \varepsilon_i \emptyset_i(r) \qquad 3.58$$

3.4 Pseudopotentials
This is a residual attraction between an ion and an electron after taking account of the effective repulsion which is as a result of the interatomic interactions. Pseudopotentials are well known to impact much in the understanding of the electronic structure of semiconductors. Empirical pseudopotentials provide the best way in understanding dielectric and optical semiconductor properties together with their energy band structures. Construction of meaningful one electron potential with its corresponding energy band structure has been made possible by the adjustments allowed by Empirical Pseudo Potential Method (EPM) to one electron potential. The EPM provides an effective and simple means of coupling the theoretical band structure to experiment work which has immediate impacts (Lu Low, Yang, Han, Fan, & Yeo, 2012). The optical properties in the high interesting semiconductors are effectively interpreted by EPM that has drawn conclusions existing to date.

The density functional theory coupling with the pseudo potentials has made a very crucial progress step in the quest of understanding electronic structure of materials. The current methods that facilitate use of pseudopotentials are vital in the examination of existing new material systems. These systems are the amorphous solids, nanoscale systems, liquids and glasses. This has made the study of systems, liquids and glasses a reality. This has made the study of both software and hardware advance and now it is possible to address systems constituting of very

many atoms hence the pseudopotential knowledge has become key special standard model for condensed matter.

The pseudopotential concept has a basis on natural spatial and energetic separation of valence and core electrons. It has allowed reduction of the computational efforts that has essential physics. The interaction of the valence and core electrons gives adequate description by the effective Hamiltonian model (Dolg, 2000). Pseudopotentials allow convenient and effective expansions of wave functions in plane waves terms best suited in describing periodical systems which has enabled their common use in band structure calculations. The pseudo potentials give an advantage as they enable reduction in the basis sets for non-periodical and molecular systems which is a crucial aspect in the study of many core electron compounds for instance transition metals.

In the density functional theory study, several ways have been developed in the generation of pseudopotentials. Some of the developed ways construct pseudopotentials for pseudo orbitals which are derived from atomic calculations and parameterized analytical pseudopotentials. Implementation of numerical integration in the solution of density functional theory, one electron equation known as the discrete variational method (DVM) is used hence does not necessarily need pseudo orbital and pseudopotential fitting by the use of any analytical function due to the direct computation of the matrix elements of the effective Hamiltonian (Rotter, 2003).

Pseudopotential development is based on inclusion of core atomic orbitals in the valence pseudo orbitals due to the reason that they produce Eigen functions to different Hamiltonians. The pseudo – wave functions allow expansion within some tractable number of plane waves which has led to high success of the ultrasoft pseudopotentials. The pseudo atoms that have the core

radii r_c have a plane wave cut off of about $\frac{2\pi}{r_c}$ which makes its construction too small when the core radius is adopted in the pseudo potential in comparison to typical inter atomic distances making the pseudo potential too hard as required. Plane waves in the description of its norm conserving wave function becomes too large. Here the elements affected are those with one radially nodeless orbital for instance 3d, 2p and 4f in the valence cell. In this case of valence states, the norm conserving pseudo valence orbital is not different from the original true orbital. At $r = 0$ both have $r' + 1$ and beyond r_c their construction is identical between r_c and 0 and are both nodeless with the same spatial norm. In these scenarios the pseudopotentials are noted to be resulting from inversion of Schrödinger equation with very strong variations in the small interval between r_c and 0 which is hard as it requires many plane waves that will correspond to wave functions.

The process of obtaining manageable pseudopotentials for the atoms, Vanderbilt led a shift from a more complicated scheme of pseudopotential that had its basis on orthonormality conditions which allowed generation of another new family smooth, reliable and of pseudopotential which can be transferred by the release of the condition of the norm conserving (Hamann, 2013). In this case the pseudopotential has the allowance of being as soft as possible in the core region to enable reduction of the plane wave cut off G_{cut} drastically. When this is applied to the study of compounds which involve rare-earth atoms and transition metals such as oxides and nitrides, it confirms its accuracy and reliability hence adopted and implemented widely despite its numerical complexity and great concepts. This makes the scheme work extremely well even to the worst cases.

The pseudopotential V_{pp} and the effective core potentials (ECP) are used to exclude atomic core electrons which are inactive from the explicit treatment in the quantum chemical calculation (Gomes & Jacob, 2012). In the corporation of the major scale relativistic effects in calculations, they are convenient and reliable techniques. The effective core potentials are derived to model core electron generated potential in an atom which enables us to obtain non-relativistic equation. It also helps in the modeling of relativistic fields and other fields such as the Hartree-Fock. The effective core potential depends on pseudo orbital transformation which is the radial node of the valence orbital being removed from the core region hence no need for base functions in the modeling of the nodes in all electron calculations (Hay and Wadt 1985).

Computation in condensed matter in conjunction with plane wave basis sets have broad areas of application due to their systematic convergence and ease of use properties. Plane waves that have a basis of General Weighted Average calculations are applied to defects, surfaces, clusters and *sp*-bonded bulk solids and their interfaces. The plane wave basis sets increases in relation to the system volume and their energy cut-off E_{cut} is necessary in description of convergence. The plane waves also have no physical description which is direct and because of this local density orbital basis sets are used instead (Zunger & Freeman, 1977). Wave function of band *n* and wave vector *k* can be expressed with reference to Fourier components $C_{nk}(G)$ where G is the reciprocal lattice vector.

$$\emptyset_{nk}(r) = \frac{1}{\sqrt{v}} \Sigma_G C_{nk}(G) exp(i(K+G).r) \qquad 3.59$$

The matrix element between unoccupied conduction $(n = c)$ and occupied valence $(n = v)$ states are defined by;

$$M_G^{vc}(kq) = \int \emptyset_{vk-q}^*(r) exp(-i(q+G).r)\emptyset_{ck}(r)dr \qquad 3.60$$

$$\sum_{G'} C^*_{vk-q}(G'-G)C_{ck}(G') \tag{3.61}$$

Independent particle polarizability is given by;

$$P^o_{GG'}(q,\omega) = \frac{2}{V}\sum_V^{occ}\sum_C^{unocc}\sum_K^{BZ} M_G^{VC}(k,q)[M_{G'}^{VC}(k,q)]^* \tag{3.62}$$

Factor 2 gives account for spin degeneracy.

Independent particle Green function together with frequency convolution which are expressed in terms of Fourier component and wave function of the screened interaction which determines the elements of the self-energy for the following summation of unoccupied and occupied states (Heather & Metiu, 1987).

$$\langle m,k|\sum(E)l,k\,|\rangle =$$

$$\frac{1}{V}\sum_n^{occ+unocc}\sum_q^{BZ}\sum_{GG'} M_G^{nl}(k,q)[M_{G'}^{nm}(k,q)]^* \times \int_{-\infty}^{\infty} \frac{exp(i\omega\delta)W_{GG'}(q,w)}{(-2\pi i)E+\omega-\epsilon_{nk-q}-i\delta\sin(\mu-\epsilon_{nk-q})}\,dw$$

$$\tag{3.63}$$

Matrix elements $M_G^{nm}(k,q)$ are generalized to arbitrary states of *m* and *n*. Matrix elements construction scales in relation to the number of plane waves used in the description of the local density approximation (LDA) wave functions. These matrix elements are determined in N_G operates where N_G is the number of plane waves that is employed to describe the plasmon-pole eigen vectors. Determination of the self-energy is done through the summation of local density approximation bands over plasmon-pole bands (Engel & Farid, 1993). The number of plasmon pole bands and local density approximation bands as well as N_{PW} and N_G have a linear increase that depends on the size of the system having the same order. Generally, the algorithm increases depending on the number of plane waves and the size of the system to the fourth order. Any

evaluation approximately of self-energy through Taylor expansions at some given sets of energies have reduction of the General Weighted Average (GWA) calculation scaling to N_{PW}^3 and give allowance of the larger GWA calculations based upon plane waves (Engel & Farid, 1993).

The pseudopotential approximation replaces the Coulomb potential in the many body Hamiltonian with smooth function which allows the electron wave functions to oscillate rapidly in the core region and are replaced by nodeless pseudo orbitals with outer range properties and right energy. The pseudo charge Z_{pp} defines the pseudo potential V_{pp} by;

$$V_{pp}(r) = \frac{-Z_{pp}(r)}{r} \hspace{6cm} 3.64$$

$$Z_{pp}(r) = f(r), r \leq r_c \hspace{5cm} 3.65$$

$$1, r > r_c' \hspace{6.5cm} 3.66$$

The cutoff radius r_c separates the core $r \leq r_c$ from valence region, $r > r_c$ of the target f(r) which is a continuous function with a constant origin value. There is agreement between pseudo wave function and one electron Hartree Fock (HF) orbital in the outer region which facilitates losing of all information of the atomic structure close to the origin. The pseudopotential affects both representation of bound orbitals and determines form of the continuum wave functions.

3.5 Self-consistent field Calculation (Scf)

Immediately after we created an input file and set it properly, we performed self-consistent field calculation. This calculation began with the construction of the beginning density that was automatically generated because there wasn't any other density in the working directory because the calculation would have started with the present density which would be wrong. The running

of self-consistent field follows the chat below. Entering the self-consistent loop, the density that is present is made use of in the construction of an effective potential which gave solutions to the Kohn-Sham equations. The resulting Eigen-functions led to the generation of new density which is properly checked and should be similar to the input density hence solution of self-consistency would have been achieved.

Self-Consistency Schematic Flow Chart
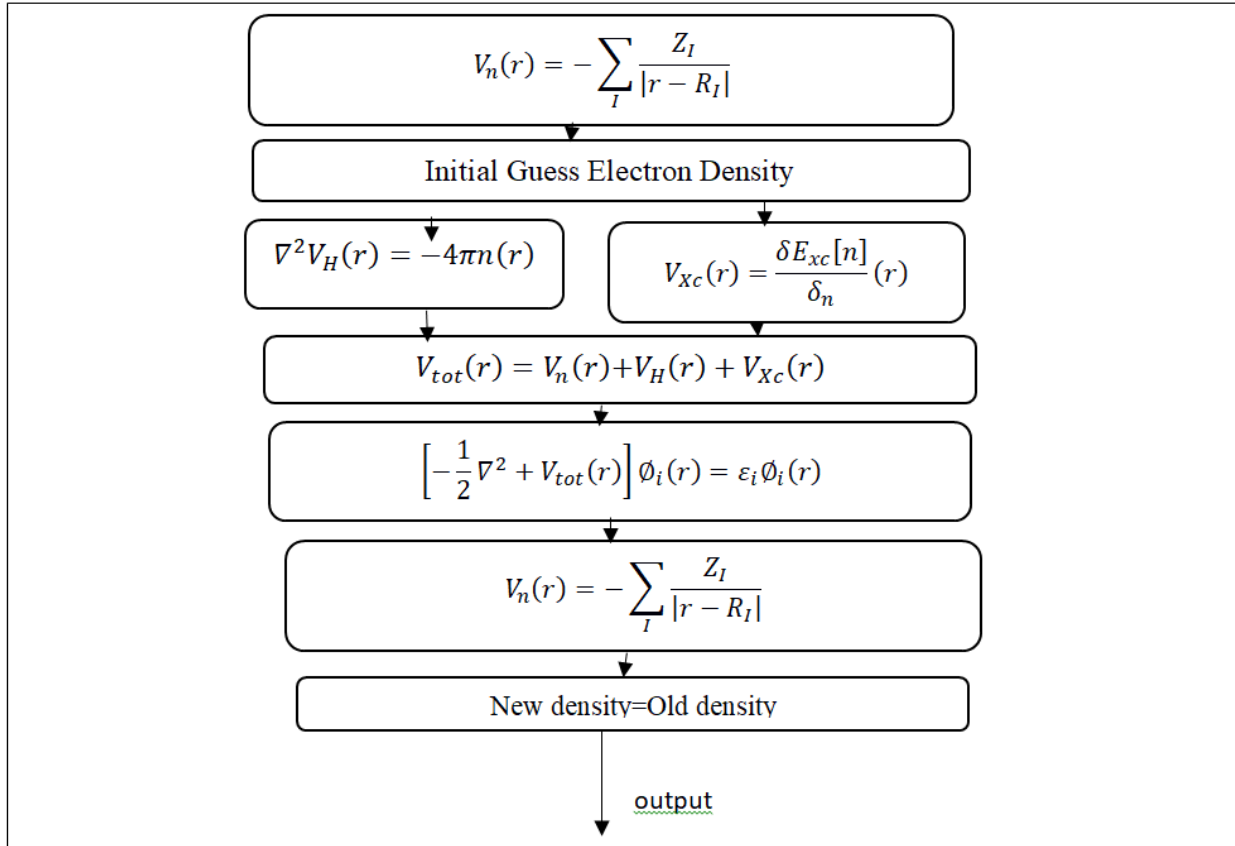
The self-consistent field loop processing is affected by the parameters present in the input file. The most crucial parameters give determination on when the program come to a controlled end. By this, one is able to define the maximum number of iterations performed and the criteria for convergence that leads to immediate stopping. Density mixing scheme configuration plays a vital role in the self-consistency calculations by specifying a general mixing procedure up to some extent the several mixing schemes give the construction of the next densities of all densities calculated.

Once self-consistency calculations has obtained the charge density, other calculations on fixed density can be performed hence non self-consistent and they include;

a) Kohn-Sham orbitals and energies for a given set of k-points.

b) Empty Kohn-Sham state calculation and increased number of computed bands Kohn-Sham energies.

c) The non-self-consistent calculations are primarily done for the computation of density of states and the plotting of the Kohn-Sham bands.

In the input file type of calculation has to be indicated for the calculation to run depending on the property under investigation i.e *scf*.

3.6 Elastic constants calculations.

The elastic constants give the measurements of the proportionality between stress of a crystal and strain provided the strain isn't so large to lead to permanent deformation of the material (Rivlin, 1948). Applying strain on the crystal and measuring strain versus the energy and determined elastic constants from the curvature of the function at zero strain. A strain is associated with a specific elastic constant combination. Cubic systems for instance diamond a basic material has three elastic constants (Bragg & Bragg, 1913) that are independent the C_{11}, C_{12}, and C_{44} one linear combination obtained by bulk modulus given as;

$$B(V) = \frac{1}{3} + 2C_{12} \qquad\qquad 3.67$$

B-bulk modulus

C_{12}-*elastic constant*

Our material at stability possess tetragonal structure. Computationally we calculated its 6 elastic constants as given as;

$C_{11}>0$, $C_{33}>0$, $C_{44}>0$, $C_{66}>0$,

$$C_{11}-C_{12}>0, \quad C_{11}+C_{33}-2C_{13}>0, \hspace{4cm} 3.68$$

$$2(C_{11}+C_{12})+C_{33}+4C_{13}>0.$$

3.7 Density of States Calculation

Calculation of density of states give description of the number of states available in a material system which are essential in the determination of energy distributions and carrier concentrations in a semiconductor (Kirsch & Metzger, 2007). Self-consistent field and non-self-consistent field calculations have to be performed before calculating the density of states. This enables production of Kohn Sham equations and creation of the required density which gives an advantage of post-processing QUANTUM ESPRESSO utility (Herath et al., 2020). Atomic charge and atomic spacing of a material in some systems allow only electrons of certain wavelength to exist. Crystalline structure of a material in other systems allow propagation of waves in one direction suppressing propagation in the other directions (Stanke & Kino, 1984). Mostly only specific states are allowed. This enables many states to be available for occupation at a given energy level with no states available at the other energy levels. Density of states of electrons at the edge of the band between conduction and valence bands of a semiconductor for instance, the increase of the electron energy enables more states to be available for occupation (Mitterbauer et al., 2003). In the other scenarios the density of states is usually discontinuous for an interval of energy an indication that no states are available in the occupation of electrons within the band gap of that given material. This condition indicates an electron at the edge of the conduction band has to lose some energy in fact at least band gap energy of that material for it to transit to the valence band (Matsui et al., 2021). This characteristic gives a determination if the material is a metal or insulator. Also conducting properties are determined by the available number of states in a band (Adler & Feinleib, 1970). For instance, for a one dimension structure

an odd number of electrons for each atom leads to half-filled top band hence there exist free electrons at Fermi level which results in a metal (Lang, 2021). The even number on the other side kills exactly whole number of the bands and others left empty. The material becomes a semi-conductor or insulator if the Fermi level will lie in the occupied band gap in between the lowest empty state and the highest occupied state (Mora-Seró & Bisquert, 2003). Density of states can be calculated for photons, phonons or electrons that can be used as a function of wave vector or energy depending on the quantum mechanical system being used. Topological properties of a material such as band structure contributes a lot in the properties of the density of states (Narang, Garcia, & Felser, 2021). Projected density of states computed the information of the different contributions of the different orbitals. Different states that contributed at different energies were noted.

Density of states are calculated in relation to the Fermi-Energy of the material by considering the vibration modes. the individual elements are studied in terms of atom vibrations.

The limitations of Density of states calculations is the absence of the states and also the phonon hardening.

3.8 Band Structure

The band structure give the description of the range of the energy levels the electrons can have along with the ranges of energy that may not have (Herman, 1955), known as forbidden bands. Band theory forms the band gaps and bands investigating the permitted quantum wave functions for electron in a very large periodic lattice of molecules and atoms. Band theory successively has been made use of in explaining very many physical properties such as optical absorption and electrical resistivity which forms the basis of the understanding of the solid state devices such as

transistors and solar cells (Arjona-Esteban et al., 2015). An isolated atom has electrons occupying atomic orbitals each having segregated energy level. When these two or more atoms come together they form a molecule with overlapping orbitals (Hoffmann, 1971). If very many such electrons from identical atoms combine to form a solid such as a crystal lattice whose atoms' atomic orbitals are overlapping with the nearby orbitals (Edmiston & Ruedenberg, 1963). Each independent energy level separates into electron levels each possessing different energy (Wannier, 1937). In a macroscopic piece whereby the number of atoms is very large also the number of orbitals become very large hence closely spaced in energy (Woodward & Hoffmann, 1969). The formation of bands is a characteristic of the valence electrons which are the outermost electrons which are involved in electrical conductivity and chemical bonding (Matta & Gillespie, 2002). The electron orbital belonging to the inner side are involved in the overlap hence exist narrowly (Gianturco, Guidotti, & Lamanna, 1972). Band gaps are the residue ranges of energy that are not occupied due to discrete widths of energy bands (Smith & Nie, 2010) (Fokin & Schreiner, 2009). The bands possess different widths depending on the degree which the atomic orbitals overlap where they are originating from (Goodenough, 1960). Bands with core orbitals for instance 2s electrons are too narrow because of the existence of small overlap between adjacent atoms. This results to large band gaps in between core bands. Higher bands contain considerably larger orbitals having more overlap which becomes wider at higher energies facilitating no existence of band gaps at higher energies (Drye, 2014).

CHAPTER FOUR

RESULTS AND DISCUSSION

At stability the compound is tetragonal and the stable structure is given below;

4.1 Crystal Structure
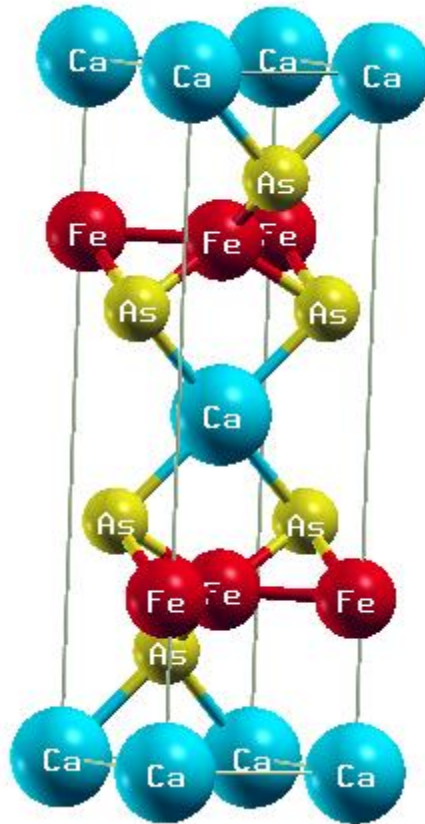
Fig 4.1: Crystal structure of $CaFe_2As_2$ as visualized from quantum espresso Xcrysden package. $a = b \neq c$

The optimized cell parameters a = 3.97 Å and c = 12.84 Å, agrees well with experimental and theoretical work as shown in Table 4.1 below. Optimization of parameters such as lattice constants and cut-off energy was done to obtain a relaxed structure free from stress (Ronning, Klimczuk, Bauer, Volz, & Thompson, 2008) (Omboga & Otieno, 2020).

The elastic properties of the iron pnictide materials give crucial information on the bonding character between the neighboring atomic planes, stability of the structure, the material's stiffness and the anisotropic type of bonding (Siryabe, Rénier, Meziane, Galy, & Castaings, 2017). Debye temperature, interatomic bonding, thermal expansion and interatomic potentials also are provided by the elastic properties (Grimvall & Sjödin, 1974). Definition of the elastic constants is done by Tylor expansion of the total energy which is the derivative of the energy as a function of lattice strain (Vitos, 2001).

Table 4.1: *Comparison of experimental and theoretical cell dimensions*

Parameter	Our work	Experimental	Theoretical	Reference
$a_0=b_0$(Å)	3.97	3.887	3.829	(Goldman, Kreyssig *et al.* 2009) (Wu, Chen *et al.* 2008)
c_0 (Å)	12.84	11.758	11.862	(Goldman, Kreyssig *et al.* 2009) (Wu, Chen *et al.* 2008)

Table 4.1 has the summary lattice parameters of our work in comparison with experimental ones. This material's optimized cell dimensions are a=3.97 and c=12.84 which are in a good agreement with related researches in ref (Samuel, Otieno, & Nyawere, 2023), ref (Carter & Britton, 1972) and ref (Winichayakul et al., 2020). Figure 4.2 reveals the band structure of this material whereby the conduction and valence bands overlap. This indicates that $CaFe_2As_2$ has high conductivity similar to that of metals. This superconductivity enables it to be one of the most important products of technology because of the growing interest in electrical systems. Figure 4.4c shows that p and s-orbitals of this material dominates the conduction band facilitating its superconductivity.

Table 4.2 below gives results of the elastic constants of $CaFe_2As_2$ as calculated and reported for the first time.

Table 4.2: *Elastic Constants of tetragonal CaFe₂As₂*

C_{ij}	GPa
C_{11}	88.86
C_{12}	22.58
C_{13}	28.63
C_{33}	63.51
C_{44}	25.93
C_{66}	31.73

Elastic constants C_{11} and C_{33} portray the level of deformation resistance along the *a*-axis and *c*-axis, respectively. Evaluated elastic constant C_{11} for $CaFe_2As_2$ is greater than that of elastic constant C_{33} by around 39.9%, a clear indication that this compound contains strong deformation resistance along the *a*-axis compared to *c*-axis.

On the other side, the elastic constant C_{44} describes the extent of shear distortion in the [1 0 0] plane, while the elastic constant C_{66} indicates the shear resistance in the [1 1 0] direction (Parvin and Naqib 2019).

This compound's elastic constants satisfy the requirement for mechanical stability conditions given by eqn. 4.14. Elastic constants C_{44} and C_{66} of $CaFe_2As_2$ obtained are 25.93 GPa and 31.73 GPa which are far less than other iron pnictides, clear indication that $CaFe_2As_2$ has a lower deformation resistance compared to other iron pnictides for instance $BaFe_2As_2$. Deformation resistance is extensively accepted as a crucial engineering property of asphalt used for surfacing

and construction of roads (Winichayakul et al., 2020). A higher deformation resistance indicates reduced potential for asphalt shearing, rutting and shoving mainly under heavy and slow-moving loads making $CaFe_2As_2$ non effective.

The Young modulus E and Poisson's ratio n and their relationships with bulk modulus and shear modulus are as tabulated in Table 4.3 below (Phani & Sanyal, 2008).

The shear anisotropic factor for the (Pai, 1995) shear planes between the <011> and <010> directions is;

$$A_1 = \frac{4C_{44}}{C_{11}+C_{55}-2C_{13}} \qquad 4.1a$$

For the (Kwak, Kim, & Bae, 2002) shear planes between <101> and <001> directions it is;

$$A_2 = \frac{4C_{55}}{C_{22}+C_{33}-2C_{23}} \qquad 4.1b$$

For the (Kwak et al., 2002) shear planes between <110> and <010> directions it is

$$A_3 = \frac{4C_{66}}{C_{11}+C_{22}-2C_{12}} \qquad 4.1c$$

But since the crystal does not have C_{22} and C_{55} our calculations of shear anisotropic factors are only for A_1 which is 1.0914 showing that the compound is anisotropic hence can withstand extreme thermal conditions.

Another important mechanical property of materials is the Vicker's hardness H_v which can be predicted by eqn. 4.1d (Gong, Wang, & Guan, 2002);

$$H_v = 0.92 \left(\frac{B}{G}\right)^{1.3137} G^{0.708} \qquad 4.1d$$

B- Bulk Modulus

G- Shear Modulus

Materials with Vicker's hardness beyond 40GPa are considered to be super hard materials. The Vicker's hardness to our compound is 18.1193GPa an indication that the compound is not hard enough to resist being dented.

Debye temperature is another basic physical property which distinguishes between low and high temperature regions for a given material. We calculated the Debye temperature for this compound by the use of the following formula (Toher et al., 2014);

$$\theta_D = \frac{h}{K_B} \left[6\pi^2 V^{\frac{1}{2}} n \right] f(\sigma) \sqrt{\frac{B_S}{M}}$$

$$\sigma = -\frac{d\epsilon_{trans}}{d\epsilon_{axial}}$$

$$f(\sigma) = \left\{ 3 \left[2 \left(\frac{2}{3} \frac{1+\sigma}{1-2\sigma} \right)^{\frac{3}{2}} + \left(\frac{1}{3} \frac{1+\sigma}{1-\sigma} \right)^{\frac{3}{2}} \right]^{-1} \right\}^{\frac{1}{3}} \qquad \text{4.1e}$$

Where *V* is the unit cell volume, *n* number of atoms in a unit cell, B_S bulky modulus, *M* molar mass, σ poisson ratio which is positive Table 4.3. The calculated Debye temperature is 3.8707K hence we expect frozen high frequency modes (Rabah, Benalia *et al*; 2010).

We have done the estimates of shear modulus (G) and bulk modulus (B) of polycrystalline aggregates from individual elastic constants, C_{ij} by Reuss and well known as voigt approximations which enables us to give the averages for the single crystal constants (Chung & Buessem, 1967).

Shear modulus indicates strength of the material unlike the bulk modulus. $G>B,$ hence $CaFe_2As_2$ mechanical failure should be corrected by application of the shear component. Bulk modulus B reveals the extent to which a material is compressible in relation to another (Mott, Dorgan, & Roland, 2008). The higher the value of B, the incompressible the material is (Mott et al., 2008). $BaFe_2As_2$ is more incompressible than $CaFe_2As_2$ with a value of 71GPa. $CaFe_2As_2$ has a value of 0.1807 for the calculated A^U and is therefore anisotropic. The Poisson's ratio (Jinyun, Yi, Lam, & Xuyong, 2010) determines ductility or brittleness of the material. The higher the ratio, the more ductile the material is, whereas a low value indicates less brittleness. For $\frac{B}{G}>1.75$ indicates ductility otherwise the material is brittle. $\frac{B}{G}$ shows that the hardness is related inversely, meaning that the smaller the ratio, the harder the material. $CaFe_2As_2$ is fairly hard and brittle with $\frac{B}{G} = 0.655935$. Poisson's ratio (n) also helps us to assess the mechanical properties of crystalline solids. Its low value indicates stability against shear (Reddy, Krishna, & Ghosh, 2010). Poisson's ratio at the same time reveals the nature of interatomic forces where a range of 0.25 and 0.50 indicates central force interaction and outside this range for non-central force interactions. Moreover, according to Poisson's ratio, materials whose ratio is less than 0.26 undergo brittle failure, but above this ratio they undergo ductile failure. Poisson's ratio of $CaFe_2As_2$ shows that it is brittle (Case, 1984). Resistance to compressive or expansive forces is measured by Young's modulus. From Table 4.3, the value of E is small, even smaller than that of $BaFe_2As_2$ of 101.6 GPa, indicating that $CaFe_2As_2$ definitely cannot withstand large tensile stress (Greaves, 2013).

Table 4.3: Mechanical properties of Bulk, Shear, Young's moduli and Poisson's ratio.

	Voigt-Reuss Approx	Reuss Approx	Voigt-Reuss Hill Average
Bulk Modulus (B) (GPa)	44.55	43.88	44.21
Young Modulus (E) (GPa)	68.39	66.40	67.40
Shear Modulus (G) (GPa)	27.48	26.60	67.40
Poisson's Ration (n)	0.24	0. 25	0.25

Cauchy pressure (Eberhart & Jones, 2012) is the difference between C_{12} and C_{44} elastic constants. This parameter reveals more about the elastic response and large density of solids. Cauchy pressure will indicate ductility or brittleness failure of crystalline solids. Cauchy pressure of both negative and positive values indicates brittleness and ductility, respectively. It also reveals chemical bonds. Positive value indicates metallic bonds while the negative one indicates covalent bonds (Haaland, 1989). In our study, the Cauchy pressure of $CaFe_2As_2$ is -3.37, indicating that our compound is brittle with covalent bonding characteristics.

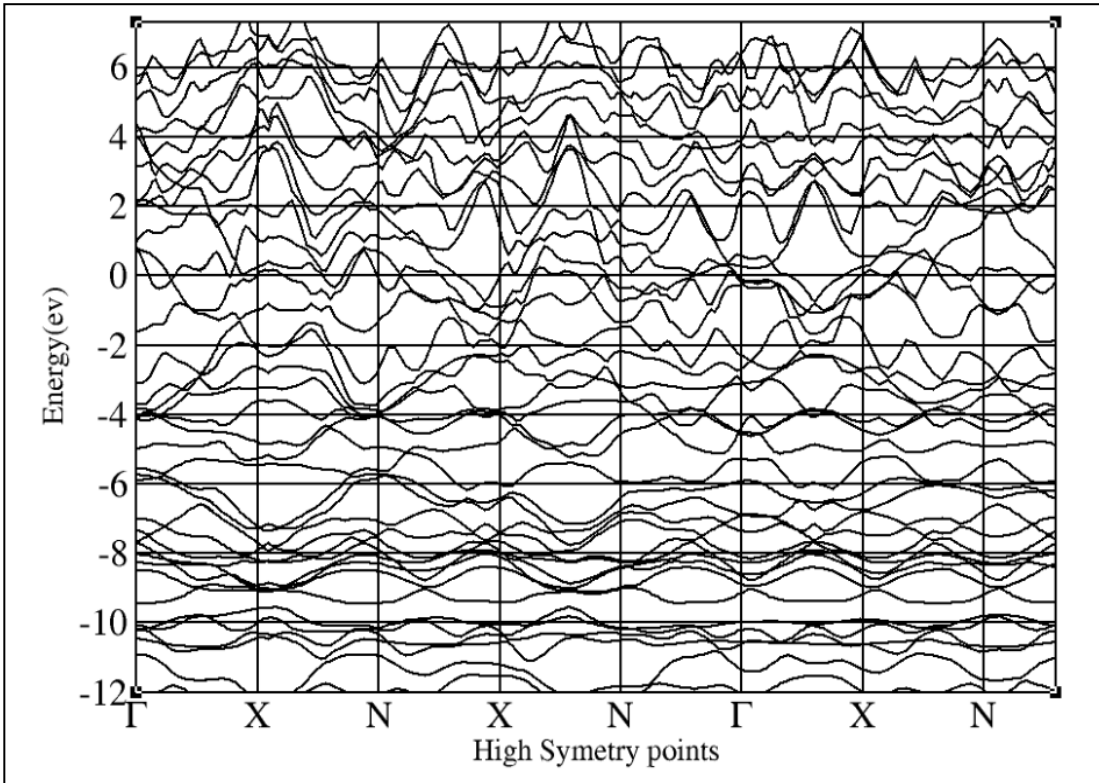## 4.1 Band Structure

Band gap is the difference in the energy between the highest point of the valence band and the lowest point of the conduction band (Jovovic & Heremans, 2008). Semiconductor materials have either indirect or direct band gap (Califano, Lu, & Zhou, 2021). A direct band gap has aligned band edges which enable electrons to transit from the valence band and conduction band without

any considerable change in momentum. In the indirect band gap the band edges are not aligned which makes it difficult for the electrons to transit directly to the conduction band .

Energy bands are categorized as filled, forbidden or mixed and empty bands (Knapp, Himpsel, & Eastman, 1979) (Cardona & Pollak, 1966). The levels of energy are occupied by the electrons which are distributed as per the Pauli exclusion principle as from the lowest energy level (Gamow, 1959) (Pauli, 1994). Electrical conductivity is facilitated by the electrons occupying the higher energy bands. The highest energy band occupied by the electrons corresponds to the valence band. The valence band is either partially or fully occupied. The empty states contribute to the electric current flow (Datta, 2004). The lowest energy band with unoccupied states is known as the conduction band. Conducting bands of materials, empty, filled or allowed states may interfere with the band gap also known as forbidden bands. The type of a material is determined by the width of the band gap; semiconductor, insulator or a metal (Escobar-Alarcón et al., 2007). At room temperature a semiconductor which gains sufficient energy to cross over the energy band gap is called intrinsic semiconductor.(Wagner, 2016)

The following are results on the band structure, density of states, and projected density of states of $CaFe_2As_2$. The band structure of $CaFe_2As_2$ calculated by the calculated energy gaps of increasing oligomer lengths is shown in Fig 4.2 was computed along high symmetry points; Γ-X-N-X-N-Γ.

Figure 4.2: Band structure of $CaFe_2As_2$.

The regions above the fermi energy at zero represent the conduction bands and those ones below represent the valence bands. High symmetry points are the local points where there are more symmetry elements that occupy this point onto itself and is the same as the Brillouin zones.

The Fermi level is the highest occupied molecular orbital at absolute temperature. It is at the center between the conduction band and the valence band, separating the particles in each band with specific quantum states from interacting (Idrissi, Ziti, Labrim, & Bahmad, 2021). From Fig 4.2, it is seen that the conduction band and valence band are overlapping, which is a clear indication that the compound is metallic and compares well with $ThCr_2As_2$ (Johrendt et al., 1997).
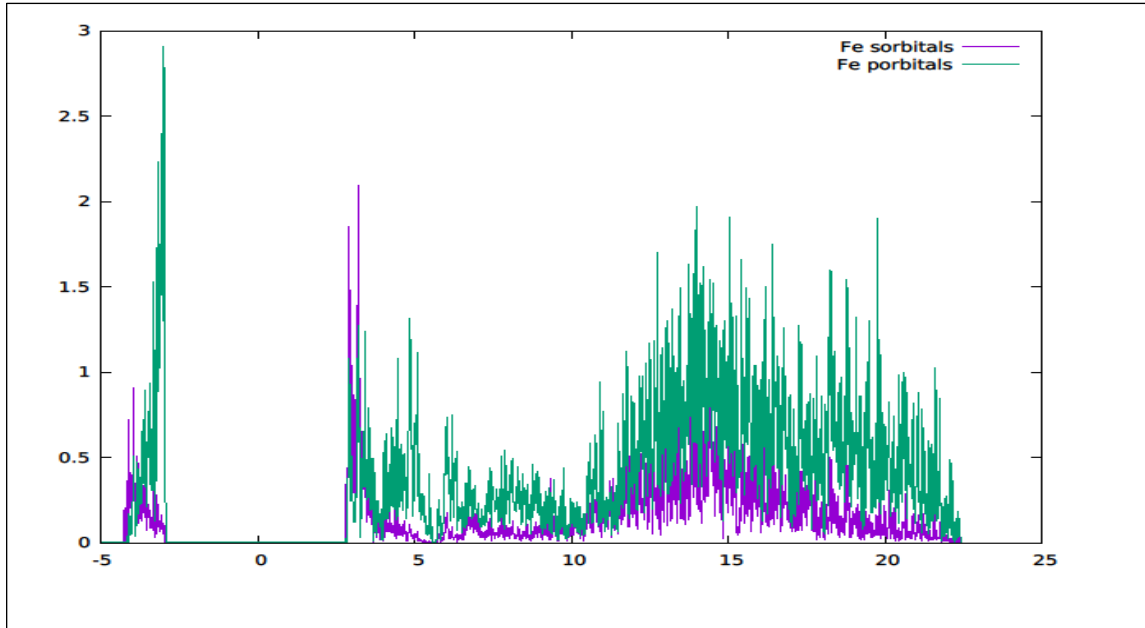
4.3 Density of States and Projected Density of States

Density of states gives numerical information on the available states at each energy level (Jelitto, 1969). The density of states is zero when there is no available state to be occupied at the energy level (Roby, 1974). Density of states with a high value corresponds to the high number of energy state to be occupied. It describes the number of states available in a system which is important in the determination of energy distributions within a semiconductor (Roby, 1974). The free motion of carriers is minimized in semiconductors to zero, one and two spatial dimensions (Yoffe, 2001) (Bergeret, Volkov, & Efetov, 2001). The density of states and the projected density of states of $CaFe_2As_2$ are shown in Fig 4.3 and Fig 4.4.
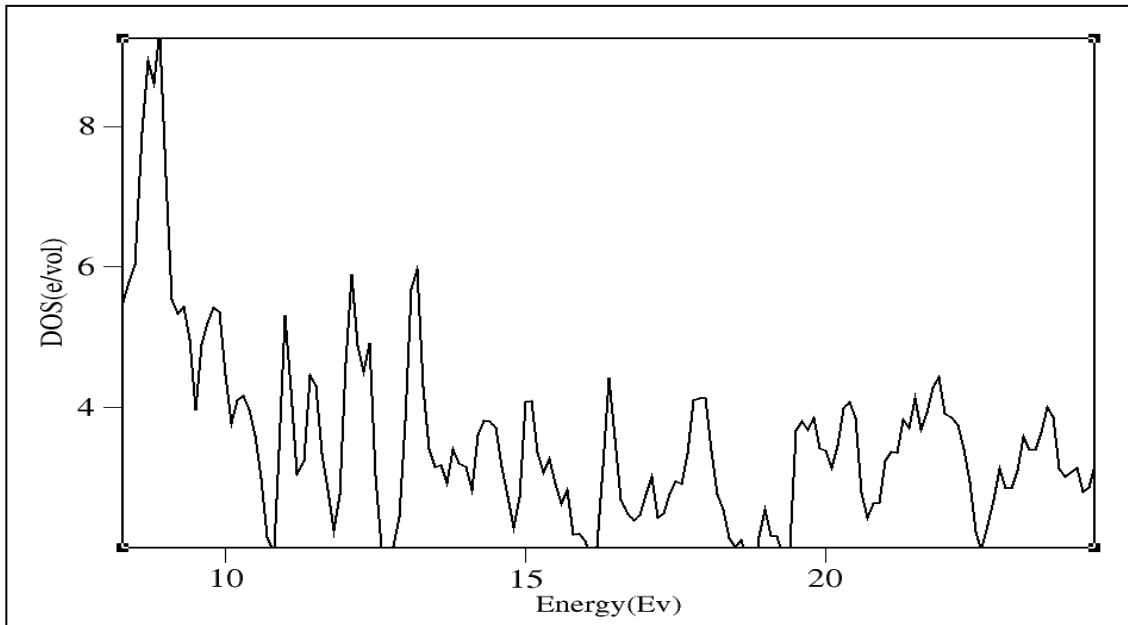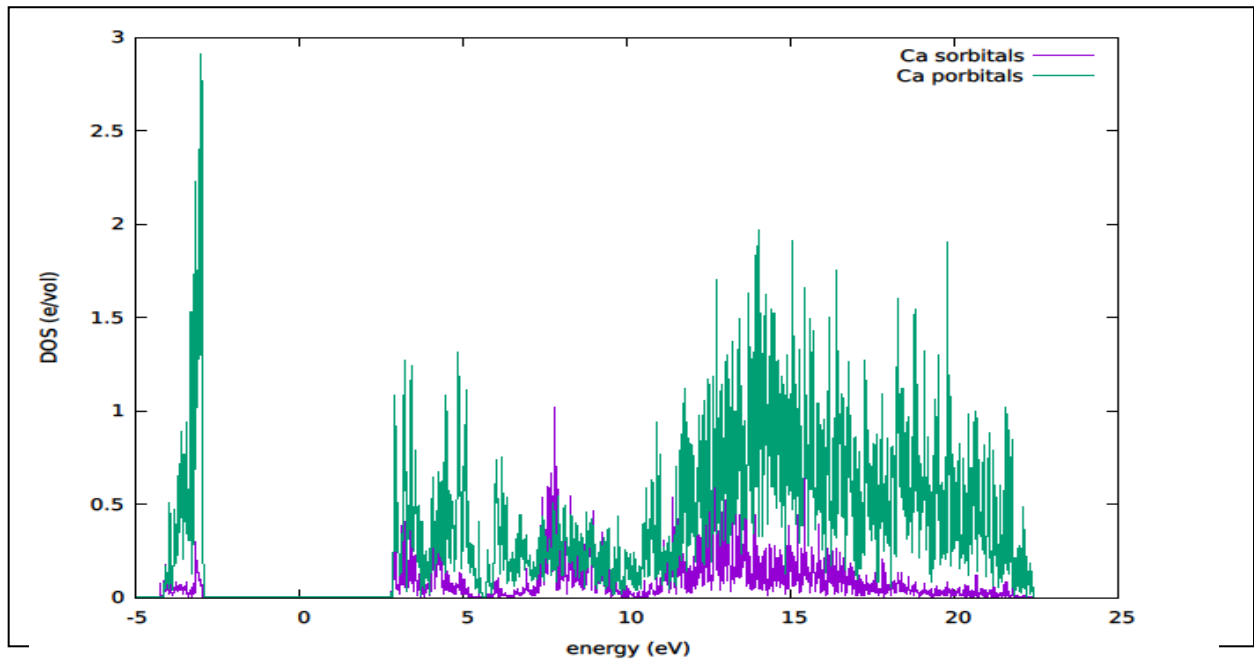

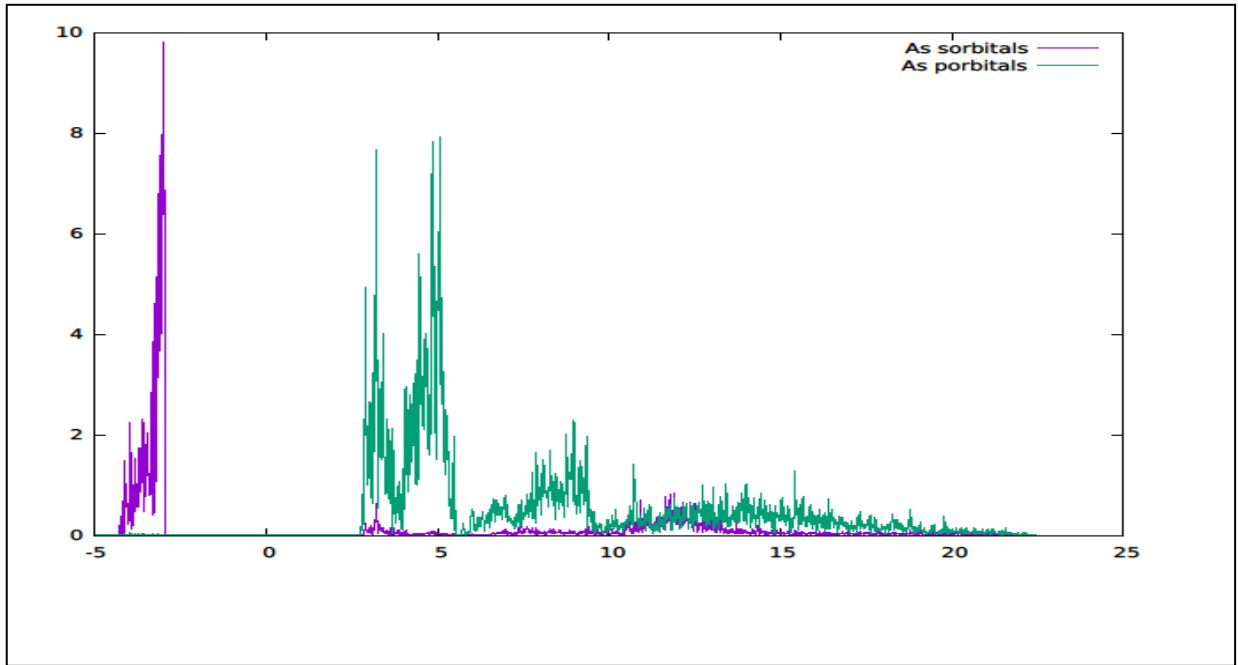**Figure 4.3**: The Density of States of $CaFe_2As_2$.

The peaks shows the vibration modes of the crystal lattice.

Figure 4.4a: The Projected Density of states of Fe p- and s-orbitals shows that they are more

dominant in the conduction band.

Figure 4.4b: The Projected Density of States of Ca p- and s-orbitals participates majorly in the

conduction band of $CaFe_2As_2$.

Figure 4.4c: The Projected Density of States of p- and s-orbitals. P-states are more dominant in the conduction band than the s-states.
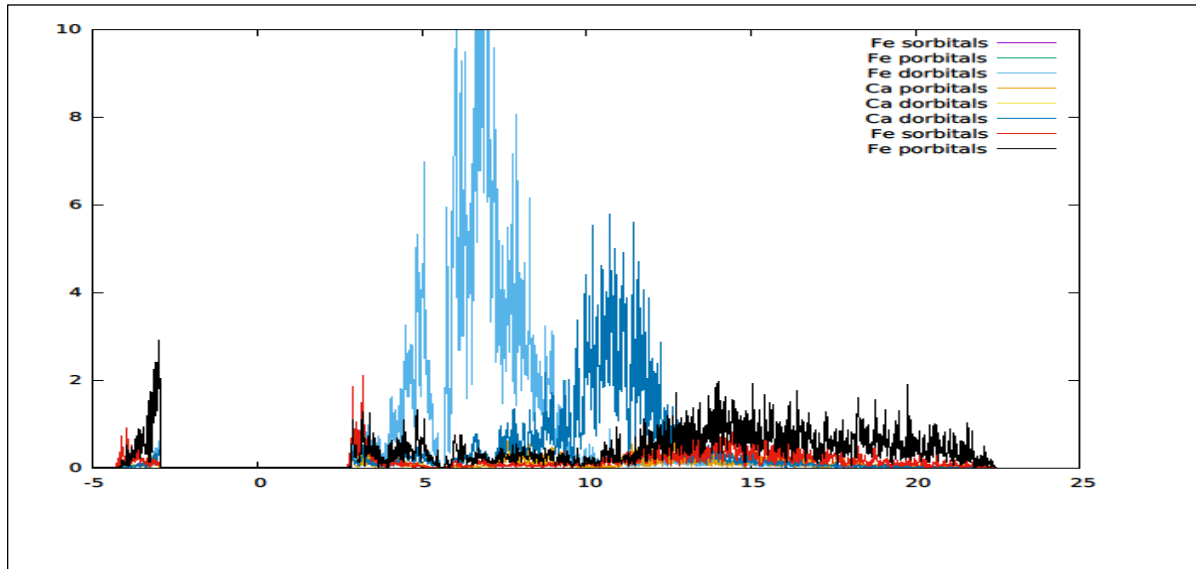
Figure 4.4d: The total Projected Density of States of orbitals for $CaFe_2As_2$.

The iron pnictide materials are formed in layered structures with charge reservoirs insulating the layers which contribute a lot in enhancing superconductivity (Bergeret et al., 2001). Iron based superconductors have a formation of constructive 2-D structure with irregular charge reservoir. For instance, at room temperature $CaFe_2As_2$ has a tetragonal structure and transit to orthorhombic upon subjection to pressure conditions.

From the angle resolved photoemission spectroscopy studies together with electronic structure calculations (Lv, Qian, & Ding, 2019), it is quite evident that the neighborhood Fermi level is made up of *Fe d* states (Fig 4.4d). *Fe 3d* states have a photoelectronic cross-section of around 10 times that of *As p* states in between the phonon energy. In Fig 4.4b, *Ca, p* also exhibits the higher binding energy between the range of -3ev and 3ev $CaFe_2As_2$ splits at *Ca* layer keeping half of the calcium atoms on each side of the split surface which shows the reconstruction hence the electronic properties of Ca are different from that of bulk *Ca*.

The contributions of *Ca, d* states are basically above the energy region with a nominal contribution at or below the energy region (J. Wang, Polleux, Lim, & Dunn, 2007). In the *Fe-d* and *As-d*, the contribution below the energy region shows a shift to the lower energies in the tetragonal phase that keeps the PDOS energy region approximately at the same energy range for both tetragonal and orthorhombic structural phases. From Fig 4.1, *Ca* layers are packed among two layers and any adjustment in *Ca* state below the energy region is as a result of the hybridization of *Ca s*-states with the electronic states attributed to *As* in the valence band(Khan et al., 2022). The compression at the c-axis as a result of the transition to the tetragonal state brought about by the subjection to an external pressure, which brings about reduction of the separation distance between *As* and *Ca* atomic layers which results in the enhancement of *Ca s* and *As p*. Even though it is evident that the contribution of *Ca* in the valence band is not much, its role in the structural change and electronic structure cannot be ignored. The *S* electrons in the cations play a key role in standardizing disorder effects and pairing interactions.

$CaFe_2As_2$ compound has a tetragonal phase as the stable phase with five atoms; one *Ca*, two *Fe*, and two *As* which upon subjection to external pressure undergoes a phase transition to the superconducting orthorhombic phase, Fig 4.5 below. Superconductivity of a material basically

means that there is no resistance and the material's flux fields are expelled from the material (Gonnella, Kaufman, & Liepe, 2016). The zero resistance in conductivity is facilitated by the lowering of temperature of a material (Liang, Yao, Wang, Liu, & Wong, 2011) (Pang, Xu, Yan, & Li, 2014) . This is well taken care of by the condition upon which we are carrying out our experiments which is at ground state temperature. The same method is applied in a superconductor in achieving superior conductivity (Lee, 2007)

In a superconductor, the conductivity happens in such a way that the electric current passed through a loop keeps on flowing without a need of a power supply (Bhattacharyya, Mitra, & Boro, 2002). We have Type I and Type II types of superconductors (Babaev & Speight, 2005). Type I has an abrupt transformation from a normal state to superconducting state at transition temperature and vice versa while Type II does not undergo abrupt transformation but partial one. Significant changes in the physical properties of a material occur for it to be transformed from non-superconducting state to superconducting state which is characterized with phase transitions. When external magnetic field is applied to a superconducting material beyond critical magnetic field point, the superconductor is transformed to normal conductor . Free energy of any conductor in the superconducting phase is lower than normal free energy in the non-superconducting phase. The properties of superconductors are advantageous for instance low power loss due to less dissipation of energy, very high speed of operation due to the zero resistance and a flow of electric current that is continuous and very high sensitivity. Superconductors are active when kept under low temperatures.

CaFe$_2$As$_2$ tetragonal stable phase undergoes a phase transition at an external pressure of 0.2GPa to the orthorhombic phase.
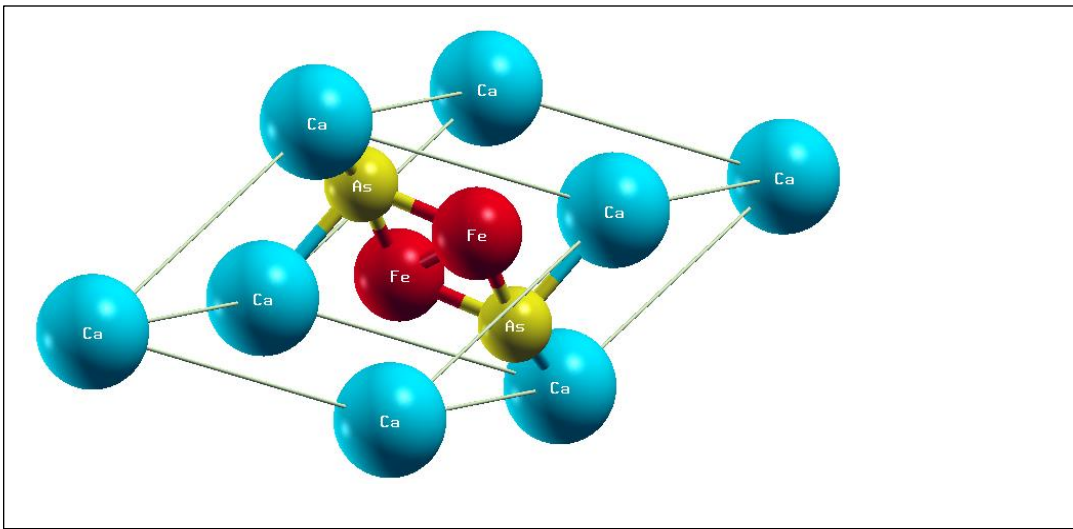
Figure 4.5*: Orthorhombic crystal structure with cell parameters $a \neq b \neq c$.

Phase transition of this compound from the stable phase tetragonal to orthorhombic occurs at ground state temperature and external pressure of 0.2GPa that happens abruptly hence confirming that it is a Type I as shown in Fig. 4.5. Phase transition occurs when the enthalpy and pressure changes are the same or nearly the same (Agora, Otieno, Nyawere, & Manyali, 2020). These two changes are indicated by two curves of different colors . Where the two lines coincide is the phase transition pressure and in this case is best at 0.2 GPa.

Pressure=0.1GPa   P = 0.2GPa   P = 0.3GPa
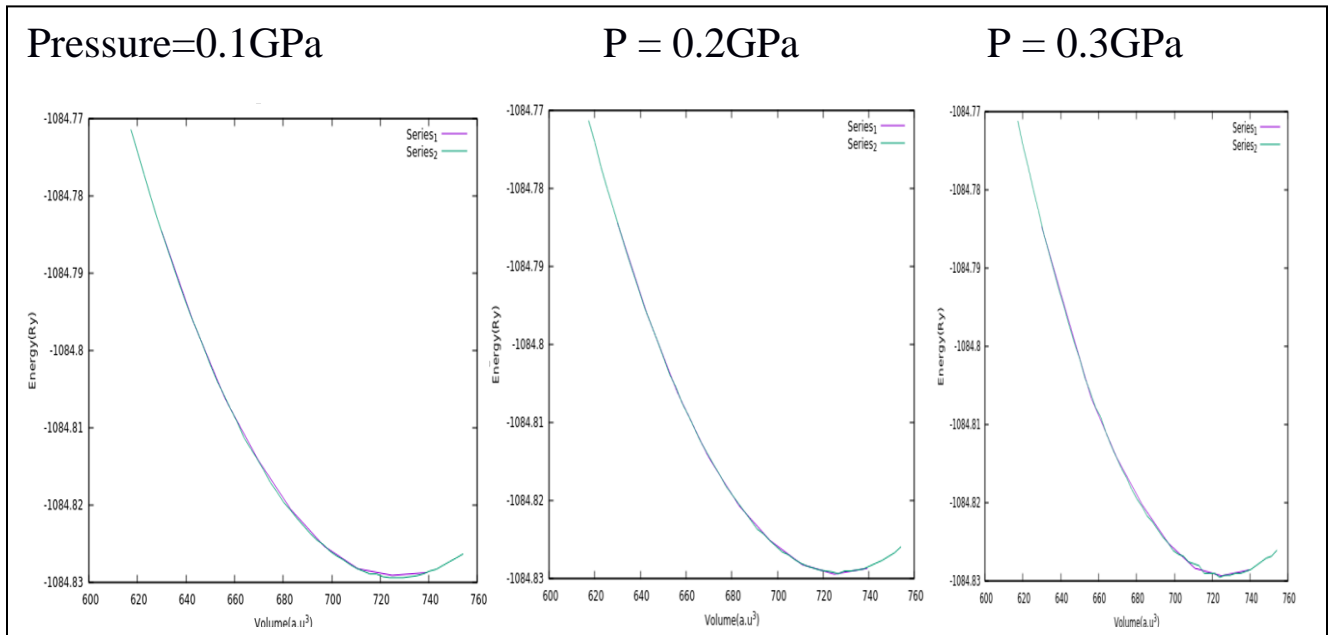
Series1- Energy, Series2- Volume

Fig 4.6: Graphs of Volume against Energy for applied Pressure of 0.1GPa, 0.2GPa and 0.3 GPa. The best fit occurs at 0.2 GPa where the two lines properly coincide.
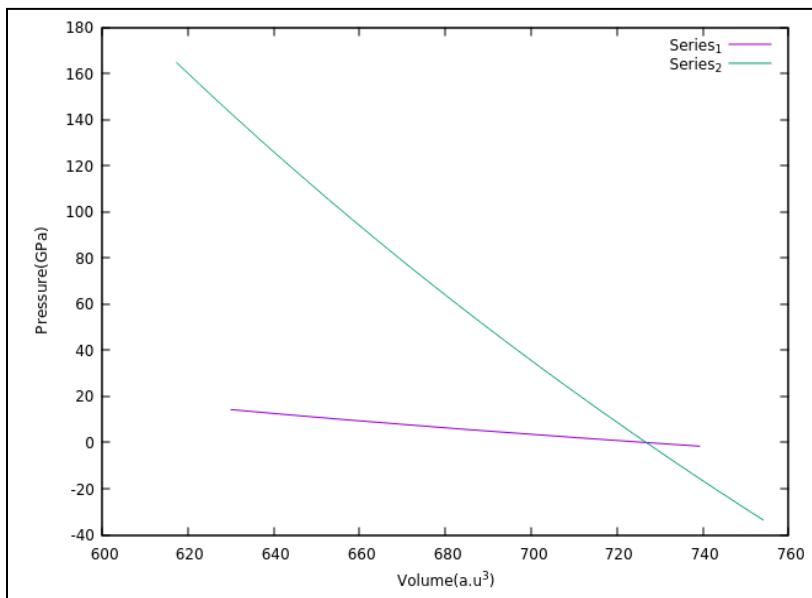
Series1- Volume

Series2- Pressure

Fig 4.7: Graph of internal pressure against internal volume at an external pressure of 0.2 GPa.

65

Heat is a form of energy and the internal energy of this material changes as heat is transferred into or out of it as shown in Fig 4.6. Before the phase transition and after, the minimum energy and the enthalpy are quite different. Fig 4.7 is in agreement with Fig 4.5 with the phase transition at 0.2GPa. This is in good agreement with the related studies showing that the pressure suppresses structural phase transition at low temperature stabilizing superconductivity (Bag et al., 2022). The product of pressure and volume enables the measurement of energy within the material even when the system does not work with the surrounding. In Fig.4.7 clearly shows the estimated transition pressure which is 0.2GPa and internal volume at about $730a.u^3$.

CHAPTER FIVE

CONCLUSIONS AND RECOMMENDATIONS

i) **Effects of Pressure on Electronic Properties**.

This research has done wide range of investigations on the effect of pressure on the mechanical and electronic properties of $CaFe_2As_2$. Additionally, we report the evaluation of the variations of the applied pressure and effects brought on the material. $CaFe_2As_2$ has not been fully exploited in terms of its properties. The material has a wide range of applications but its properties need to be enhanced by the subjection of external change of conditions. In coming up with well-presented results in the previous chapter, we employed the use of *Ab initio* studies on materials which makes use of material computation in the explicit study of materials.

$CaFe_2As_2$ has a body centered tetragonal crystal structure at room temperature with a space group of *14/mmm* and lattice parameters along the three axes of $3.97A^o$, $b = 3.97A^o$, $c = 12.84A^o$ given in Fig.4.1. This material has all its angles equal to 90° with side *a* equal to side *b*. After external application of pressure which facilitates its phase transition from tetragonal to body centered orthorhombic, the material contains lattices of all angle equal with all its sides unequal. The material is well described by these three lattice parameters. The material's crystal structure is defined by the unit cell. The unit cell is the smallest repeated unit that has a full crystal structure symmetry. In the unit cell coordinates are used in the expression of the atomic arrangement. The structure has $CaFe_2As_2$ *Ca* confined between *Fe-As* along the c-axis. The tetrahedral Fe-As are the usual structural units to the 122 class of iron pnictides AFe_2As_2 and the oxypnictides RFeAsO superconductors.

In Fig.4.2 is a graph that shows the calculated density of states (DOS) of this compound at tetragonal stable phase. There are many existing separated energy regions on the figure which we

attribute to *As* s-orbitals shallow core levels and valence electronic states. In the valence band we observe hybridization between *As* s-orbitals and *Fe* p-orbitals. Valence electrons in the neighborhood of Fermi level essentially contained Fe d-states. Fe-As hybridization results to *As* p-states finite contribution of *Ca* s-orbitals is found to be significant. This indicates that even though the *Fe* p-orbital and s-orbital states dominate the role of electronic properties of $CaFe_2As_2$ the other orbitals contribute and are non-zeros because of the covalence between the states.

Crystal is rigid on [1 0 0] and [0 1 0] in consideration of uniaxial stress, which indicates the strength of bonds in the individual points of the material. Using Poisson ratio in comparison with bulk, the shear and Young moduli in consideration of interatomic forces confirms that our material is brittle.

ii)   Effects of pressure on Mechanical Properties.

In comparison, $CaFe_2As_2$ with $BaFe_2As_2$ these compounds belong to the same space group. $CaFe_2As_2$ has much smaller lattice parameters compared to $BaFe_2As_2$. The average bond lengths of this material for instance the *Ca-As* bond is much smaller as compared with *Ba-As* bond. This clearly indicates that *Ca* layer and *FeAs* layer interaction is so much stronger that of *Ba* layer with *FeAs* layer due to high forces of attraction. Most material's electronic structure is highly sensitive to the changes in the crystal structure as various electronic states hybridization has high dependence on bond length, deformation of the lattice structure that brings about change bond angles. It is identified that covalency causes key interactions which leads to the deformation of the crystal structures which brings forth ground state properties (Sypek 2019).

Cauchy pressure, which is the difference of elastic constants, reveals elastic response. $CaFe_2As_2$ gives a negative value, hence indicating that it is brittle with covalent bonding characteristics.

For determining whether our material is anisotropic, calculation using the lattice parameters of our material, it indicated that it is isotropic just like its parent compound $ThCr_2Si_2$. Band structure shows that $CaFe_2As_2$, is metallic a property that enhances its superconductivity.

iii)   Effects of varying pressure on phase change.

$CaFe_2As_2$ is an interesting material as it exhibits a rich pressure-temperature phase diagrams which provides an effective avenue to study the interplay between superconductivity and magnetism in the *Fe* based pnictide compounds where superconductivity is driven by magnetic fluctuations. At ground state temperature tetragonal stable phase $CaFe_2As_2$ at some applied pressure of 0.2GPa undergoes a concomitant phase change to orthorhombic phase. The 0.2GPa applied pressure brought about both magnetic and structural transitions whereby magnetism is suppressed and the new transition emerges with no magnetic order. The applied pressure brought about occupation of the holes in the compound by the electrons hence superconductivity achieved by the hole or electron doping (Lv, Deng *et al*; 2011). The elimination of high temperature transition of the 111 and 122 iron pnictides is the basic necessity for emergence of superconductivity in these materials (Liu, Palczewski *et al*; 2011). It has been discovered that application of modest pressure leads to the suppression of the first order structural phase change. Over some limited amount of pressure application, superconductivity emerges which can in turn be suppressed which potentially high temperature phase. Pressure is a parameter made use in the tuning superconductivity behavior of these iron based compounds (Gati, Xiang *et al*; 2020). This confirms strong interaction between magnetic degrees of freedom, superconductivity and lattice in AFe_2As_2class. For instance magnetic frustration yields spin fluctuations in doped compounds which plays a critical role in superconductivity phases.

Pressure induced effects in the 122 class of iron pnictides has been investigated and emergence of superconductivity potentialities have been evaluated at different ranges of conditions of pressure and temperature. For superconductivity in $SrFe_2As_2$ and $BaFe_2As_2$ containing the alkaline earth metals larger than *Ca* is identified at fairly high pressures of 3.2GPa and 4GPa respectively (Till, Grove *et al*; 2012) with transition temperature of about 27K and 29K. $CaFe_2As_2$ on the other side shows superconductivity with transition temperature of 12K at lower pressures between 0.2GPa and 0.9GP (Johnston, Abdel-Hafiez *et al*; 2014) as the small atomic size of *Ca* employs less strain. Current research underground state temperature confirms the range of pressure applied for superconductivity to emerge in this material by taking the lower limit because of the constant room temperature.

In Fig.4.5 we observe that the transition to orthorhombic antiferromagnetic phase is suppressed upon increasing pressure and disappear above pressure of 0.3GPa an indication of emergence of collapsed tetragonal phase. The result showing the absence of superconductivity exhibits sharp transitions in the pressure range which involves transitions from tetragonal to orthorhombic, orthorhombic to collapsed tetragonal and tetragonal to collapsed tetragonal phases. Superconductivity is identified at a pressure where the compound is in the proximity of the transition to collapsed tetragonal phase. The origin of superconductivity in the material thus appears to have a relation with the multi-crystallographic phases in between the intermediate pressure.

The material undergoes a structural phase change at an external pressure of 0.2GPa from the tetragonal stable phase to orthorhombic at ground state temperature. This makes the material a good superconductor. The material is isotropic with uniformity of properties at all directions and this enables it to be used as the crystals with cubic symmetry.

SUGGESTION FOR FURTHER RESEARCH

Investigate the effects of pressure and doping on the superconducting properties of iron pnictides, specifically examining how variations in these two factors influence the critical temperature and other relevant characteristics.

REFERENCES

Adler, D., & Feinleib, J. (1970). Electrical and optical properties of narrow-band materials. *Physical Review B, 2*(8), 3112.

Agora, J. O., Otieno, C., Nyawere, P. W., & Manyali, G. S. (2020). Ab initio study of pressure induced phase transition, structural and electronic structure properties of superconducting perovskite compound GdBa2Cu3O7-x. *Computational Condensed Matter, 23*, e00461.

Aichinger, M., & Krotscheck, E. (2005). A fast configuration space method for solving local Kohn–Sham equations. *Computational materials science, 34*(2), 188-212.

Arjona-Esteban, A., Krumrain, J., Liess, A., Stolte, M., Huang, L., Schmidt, D., . . . Meerholz, K. (2015). Influence of solid-state packing of dipolar merocyanine dyes on transistor and solar cell performances. *Journal of the American Chemical Society, 137*(42), 13524-13534.

Babaev, E., & Speight, M. (2005). Semi-Meissner state and neither type-I nor type-II superconductivity in multicomponent superconductors. *Physical Review B, 72*(18), 180502.

Bag, B., Loke, R., Singh, B., Thamizhavel, A., Singh, B., & Ramakrishnan, S. (2022). Superconductivity in Heusler compound ScAu2Al. *Journal of physics: Condensed matter, 34*(19), 195403.

Bartalesi, A. (2010). Design of high field solenoids made of high temperature superconductors: Fermi National Accelerator Lab.(FNAL), Batavia, IL (United States).

Bergeret, F., Volkov, A., & Efetov, K. (2001). Enhancement of the Josephson current by an exchange field in superconductor-ferromagnet structures. *Physical review letters, 86*(14), 3140.

Bhattacharyya, B., Mitra, S., & Boro, A. (2002). Electrochemical machining: new possibilities for micromachining. *Robotics and Computer-Integrated Manufacturing, 18*(3-4), 283-289.

Biswal, G., & Mohanta, K. (2021). A recent review on iron-based superconductor. *Materials Today: Proceedings, 35*, 207-215.

Bragg, W. H., & Bragg, W. L. (1913). The structure of the diamond. *Proceedings of the Royal Society of London. Series A, Containing Papers of a Mathematical and Physical Character, 89*(610), 277-291.

Bridgman, P. W. (1964). The compressibility and pressure coefficient of resistance of ten elements *Papers 59-93* (pp. 2175-2194): Harvard University Press.

Buongiorno, J., Venerus, D. C., Prabhat, N., McKrell, T., Townsend, J., Christianson, R., . . . Alvarado, J. L. (2009). A benchmark study on the thermal conductivity of nanofluids. *Journal of Applied Physics, 106*(9).

Califano, M., Lu, R., & Zhou, Y. (2021). Indirect to Direct Band Gap Transformation by Surface Engineering in Semiconductor Nanostructures. *ACS nano, 15*(12), 20181-20191.

Canfield, P., Bud'ko, S., Ni, N., Kreyssig, A., Goldman, A., McQueeney, R., . . . Yu, W. (2009). Structural, magnetic and superconducting phase transitions in CaFe2As2 under ambient and applied pressure. *Physica C: Superconductivity, 469*(9-12), 404-412.

Cardona, M., & Pollak, F. H. (1966). Energy-band structure of germanium and silicon: The k· p method. *Physical Review, 142*(2), 530.

Caro, A., & Victoria, M. (1989). Ion-electron interaction in molecular-dynamics cascades. *Physical Review A, 40*(5), 2287.

Carter, V. B., & Britton, D. (1972). The crystal structures of 2, 4, 6-trichlorobenzonitrile and 2, 4, 6-tribromobenzonitrile. *Acta Crystallographica Section B: Structural Crystallography and Crystal Chemistry, 28*(3), 945-950.

Case, E. (1984). The effect of microcracking upon the Poisson's ratio for brittle materials. *Journal of materials science, 19*, 3702-3712.

Chang, Y., Hsu, F., Kirchner, S., Mou, C., Lee, T., & Chung, C.-H. (2019). Strange superconductivity near an antiferromagnetic heavy-fermion quantum critical point. *Physical Review B, 99*(9), 094513.

Chetyrkin, K. G., & Tkachov, F. V. (1981). Integration by parts: the algorithm to calculate β-functions in 4 loops. *Nuclear Physics B, 192*(1), 159-204.

Chiang, Y. N., Dzyuba, M., Shevchenko, O., & Vasiliev, A. (2012). Conductance of non-ballistic point contacts in hybrid systems "normal metal/superconductor" Cu/Mo–C and Cu/LaOFFeAs. *Physica C: Superconductivity, 483*, 149-155.

Chu, C., & Lorenz, B. (2009). High pressure studies on Fe-pnictide superconductors. *Physica C: Superconductivity, 469*(9-12), 385-395.

Chung, D., & Buessem, W. (1967). The voigt-reuss-hill approximation and elastic moduli of polycrystalline MgO, CaF2, β-ZnS, ZnSe, and CdTe. *Journal of Applied Physics, 38*(6), 2535-2540.

Conti, I., Cerullo, G., Nenov, A., & Garavelli, M. (2020). Ultrafast spectroscopy of photoactive molecular systems from first principles: Where we stand today and where we are going. *Journal of the American Chemical Society, 142*(38), 16117-16139.

da Jornada, F. H., Qiu, D. Y., & Louie, S. G. (2017). Nonuniform sampling schemes of the Brillouin zone for many-electron perturbation-theory calculations in reduced dimensionality. *Physical Review B, 95*(3), 035109.

Datta, S. (2004). Electrical resistance: an atomistic view. *Nanotechnology, 15*(7), S433.

David, P. A. (1991). The hero and the herd in technological history: Reflections on Thomas Edison and the battle of the systems. *Favorites to Fortune*, 72-119.

Dolg, M. (2000). Effective core potentials. *Modern methods and algorithms of quantum chemistry, 3*, 507-540.

Dragomir, I., & Ungár, T. (2002). The dislocations contrast factors of cubic crystals in the Zener constant range between zero and unity. *Powder Diffraction, 17*(2), 104-111.

Drye, T. (2014). *Structural changes and the nature of superconductivity in rare-earth doped CaFe 2 As 2.* University of Maryland, College Park.

Eberhart, M. E., & Jones, T. E. (2012). Cauchy pressure and the generalized bonding model for nonmagnetic bcc transition metals. *Physical Review B, 86*(13), 134106.

Edmiston, C., & Ruedenberg, K. (1963). Localized atomic and molecular orbitals. *Reviews of Modern Physics, 35*(3), 457.

Engel, G., & Farid, B. (1993). Generalized plasmon-pole model and plasmon band structures of crystals. *Physical Review B, 47*(23), 15931.

Escobar-Alarcón, L., Arrieta, A., Camps, E., Muhl, S., Rodil, S., & Vigueras-Santiago, E. (2007). An alternative procedure for the determination of the optical band gap and thickness of amorphous carbon nitride thin films. *Applied surface science, 254*(1), 412-415.

Fokin, A. A., & Schreiner, P. R. (2009). Band gap tuning in nanodiamonds: first principle computational studies. *Molecular Physics, 107*(8-12), 823-830.

Gamow, G. (1959). The exclusion principle. *Scientific American, 201*(1), 74-90.

Giannozzi, P., Andreussi, O., Brumme, T., Bunau, O., Nardelli, M. B., Calandra, M., . . . Cococcioni, M. (2017). Advanced capabilities for materials modelling with Quantum ESPRESSO. *Journal of physics: Condensed matter, 29*(46), 465901.

Gianturco, F., Guidotti, C., & Lamanna, U. (1972). Electronic Properties of Sulphur Hexafluoride. II. Molecular Orbital Interpretation of Its X-Ray Absorption Spectra. *The Journal of Chemical Physics, 57*(2), 840-846.

Gomes, A. S. P., & Jacob, C. R. (2012). Quantum-chemical embedding methods for treating local electronic excitations in complex chemical systems. *Annual Reports Section" C"(Physical Chemistry), 108*, 222-277.

Gong, J., Wang, J., & Guan, Z. (2002). A comparison between Knoop and Vickers hardness of silicon nitride ceramics. *Materials Letters, 56*(6), 941-944.

Gonnella, D., Kaufman, J., & Liepe, M. (2016). Impact of nitrogen doping of niobium superconducting cavities on the sensitivity of surface resistance to trapped magnetic flux. *Journal of Applied Physics, 119*(7).

Goodenough, J. B. (1960). Band structure of transition metals and their alloys. *Physical Review, 120*(1), 67.

Greaves, G. N. (2013). Poisson's ratio over two centuries: challenging hypotheses. *Notes and Records of the Royal Society, 67*(1), 37-58.

Grimvall, G., & Sjödin, S. (1974). Correlation of properties of materials to Debye and melting temperatures. *Physica Scripta, 10*(6), 340.

Haaland, A. (1989). Covalent versus dative bonds to main group metals, a useful distinction. *Angewandte Chemie International Edition in English, 28*(8), 992-1007.

Halkier, A., Helgaker, T., Jørgensen, P., Klopper, W., Koch, H., Olsen, J., & Wilson, A. K. (1998). Basis-set convergence in correlated calculations on Ne, N2, and H2O. *Chemical Physics Letters, 286*(3-4), 243-252.

Hamann, D. (2013). Optimized norm-conserving Vanderbilt pseudopotentials. *Physical Review B, 88*(8), 085117.

Harrison, W. A. (1985). Coulomb interactions in semiconductors and insulators. *Physical Review B, 31*(4), 2121.

Heather, R., & Metiu, H. (1987). An efficient procedure for calculating the evolution of the wave function by fast Fourier transform methods for systems with spatially extended wave function and localized potential. *The Journal of Chemical Physics, 86*(9), 5009-5017.

Hedin, L., & Lundqvist, B. I. (1971). Explicit local exchange-correlation potentials. *Journal of Physics C: Solid state physics, 4*(14), 2064.

Herath, U., Tavadze, P., He, X., Bousquet, E., Singh, S., Muñoz, F., & Romero, A. H. (2020). PyProcar: A Python library for electronic structure pre/post-processing. *Computer Physics Communications, 251*, 107080.

Herman, F. (1955). The electronic energy band structure of silicon and germanium. *Proceedings of the IRE, 43*(12), 1703-1732.

Hoffmann, R. (1971). Interaction of orbitals through space and through bonds. *Accounts of Chemical Research, 4*(1), 1-9.

Hosoi, S., Matsuura, K., Ishida, K., Wang, H., Mizukami, Y., Watashige, T., . . . Shibauchi, T. (2016). Nematic quantum critical point without magnetism in FeSe1− x S x superconductors. *Proceedings of the National Academy of Sciences, 113*(29), 8139-8143.

Huang, H., Fan, X., Singh, D. J., & Zheng, W. (2020). Recent progress of TMD nanomaterials: phase transitions and applications. *Nanoscale, 12*(3), 1247-1268.

Hufenbach, W., Böhm, R., Thieme, M., Winkler, A., Mäder, E., Rausch, J., & Schade, M. (2011). Polypropylene/glass fibre 3D-textile reinforced composites for automotive applications. *Materials & Design, 32*(3), 1468-1476.

Idrissi, S., Ziti, S., Labrim, H., & Bahmad, L. (2021). Band gaps of the solar perovskites photovoltaic CsXCl3 (X= Sn, Pb or Ge). *Materials Science in Semiconductor Processing, 122*, 105484.

Jelitto, R. J. (1969). The density of states of some simple excitations in solids. *Journal of Physics and Chemistry of Solids, 30*(3), 609-626.

Jin, Y., Zhang, T., Pan, N., Wang, S., Zhang, B., Zhu, X., . . . Zhang, M. (2022). Surface functionalization of carbon cloth with conductive Ni/Fe-MOFs for highly efficient oxygen evolution. *Surfaces and Interfaces, 33*, 102294.

Jinyun, Z., Yi, L., Lam, J., & Xuyong, C. (2010). The Poisson ratio and modulus of elastic knitted fabrics. *Textile Research Journal, 80*(18), 1965-1969.

Johrendt, D., Felser, C., Jepsen, O., Andersen, O. K., Mewis, A., & Rouxel, J. (1997). LMTO band structure calculations of ThCr2Si2-type transition metal compounds. *Journal of solid state chemistry, 130*(2), 254-265.

Josephson, R. (1993). Contraction dynamics and power output of skeletal muscle. *Annual review of physiology, 55*(1), 527-546.

Jovovic, V., & Heremans, J. (2008). Measurements of the energy band gap and valence band structure of AgSbTe 2. *Physical Review B, 77*(24), 245204.

Katayama, N., Matsubayashi, K., Nomura, Y., Ji, S., Leao, J., Green, M., . . . Yamada, K. (2012). Conductivity and incommensurate antiferromagnetism of Fe1. 02Se0. 10Te0. 90 under pressure. *Europhysics Letters, 98*(3), 37002.

Kawashima, K., Ishida, S., Fujihisa, H., Gotoh, Y., Yoshida, Y., Eisaki, H., . . . Iyo, A. (2018). Superconductivity in a 122-type Fe-based compound (La, Na, K) Fe 2 As 2. *Scientific Reports, 8*(1), 16827.

Khan, A. A., Saqib, M., Zada, Z., Chahed, F., Ismail, M., Ishaq, M., . . . Faizan, M. (2022). Electronic structure, magnetic, and thermoelectric properties of BaMn2As2 compound: A first-principles study. *Physica Scripta, 97*(6), 065810.

Kirsch, W., & Metzger, B. (2007). The Integrated Density of States. *Spectral Theory and Mathematical Physics: A Festschrift in Honor of Barry Simon's 60th Birthday, 76*, 649.

Knapp, J., Himpsel, F., & Eastman, D. (1979). Experimental energy band dispersions and lifetimes for valence and conduction bands of copper using angle-resolved photoemission. *Physical Review B, 19*(10), 4952.

Kohori, Y., Yamato, Y., Iwamoto, Y., & Kohara, T. (2000). Appearance of anisotropic non s-wave superconductivity above the critical pressure of antiferromagnetic CeRhIn5: 115In nuclear quadrupole resonance study. *The European Physical Journal B-Condensed Matter and Complex Systems, 18*(4), 601-604.

Kresse, G., & Joubert, D. (1999). From ultrasoft pseudopotentials to the projector augmented-wave method. *Physical Review B, 59*(3), 1758.

Kristyan, S. (2008). Properties of the multi-electron densities "between" the Hohenberg–Kohn theorems and variational principle. *Journal of Molecular Structure: THEOCHEM, 858*(1-3), 1-11.

Kutzelnigg, W., Del Re, G., & Berthier, G. (1968). Correlation coefficients for electronic wave functions. *Physical Review, 172*(1), 49.

Kwak, T., Kim, Y., & Bae, W. (2002). Finite element analysis on the effect of die clearance on shear planes in fine blanking. *Journal of Materials Processing Technology, 130*, 462-468.

Lang, P. F. (2021). Fermi energy, metals and the drift velocity of electrons. *Chemical Physics Letters, 770*, 138447.

Lee, P. A. (2007). From high temperature superconductivity to quantum spin liquid: progress in strong correlation physics. *Reports on Progress in Physics, 71*(1), 012501.

Levämäki, H., Tian, L.-Y., Vitos, L., & Ropo, M. (2019). An automated algorithm for reliable equation of state fitting of magnetic systems. *Computational materials science, 156*, 121-128.

Liang, Q., Yao, X., Wang, W., Liu, Y., & Wong, C. P. (2011). A three-dimensional vertically aligned functionalized multilayer graphene architecture: an approach for graphene-based thermal interfacial materials. *ACS nano, 5*(3), 2392-2401.

Liu, J., & Liang, W. (2011). Analytical Hessian of electronic excited states in time-dependent density functional theory with Tamm-Dancoff approximation. *The Journal of Chemical Physics, 135*(1).

Lu Low, K., Yang, Y., Han, G., Fan, W., & Yeo, Y.-C. (2012). Electronic band structure and effective mass parameters of Ge1-xSnx alloys. *Journal of Applied Physics, 112*(10).

Lv, B., Qian, T., & Ding, H. (2019). Angle-resolved photoemission spectroscopy and its application to topological materials. *Nature Reviews Physics, 1*(10), 609-626.

Marini, A., Poncé, S., & Gonze, X. (2015). Many-body perturbation theory approach to the electron-phonon interaction with density-functional theory as a starting point. *Physical Review B, 91*(22), 224310.

Matsui, F., Makita, S., Matsuda, H., Nakamura, E., Okano, Y., Yano, T., . . . Suga, S. (2021). Valence Band Dispersion Embedded in Resonant Auger Electrons. *Journal of the Physical Society of Japan, 90*(12), 124710.

Matta, C., & Gillespie, R. (2002). Understanding and interpreting molecular electron density distributions. *Journal of Chemical Education, 79*(9), 1141.

Mazzi, F., Galli, E., & Gottardi, G. (1976). The crystal structure of tetragonal leucite. *American Mineralogist, 61*(1-2), 108-115.

Meier, W. R. (2018). *Growth, Properties and Magnetism of CaKFe 4 As 4.* Iowa State University.

Mitterbauer, C., Kothleitner, G., Grogger, W., Zandbergen, H., Freitag, B., Tiemeijer, P., & Hofer, F. (2003). Electron energy-loss near-edge structures of 3d transition metal oxides recorded at high-energy resolution. *Ultramicroscopy, 96*(3-4), 469-480.

Miyamoto, T., Minase, G., Shin, T., Ueda, H., Okada, H., & Sengoku, K. (2017). Human male infertility and its genetic causes. *Reproductive medicine and biology, 16*(2), 81-88.

Mora-Seró, I., & Bisquert, J. (2003). Fermi level of surface states in TiO2 nanoparticles. *Nano Letters, 3*(7), 945-949.

Mott, P. H., Dorgan, J. R., & Roland, C. (2008). The bulk modulus and Poisson's ratio of "incompressible" materials. *Journal of Sound and Vibration, 312*(4-5), 572-575.

Narang, P., Garcia, C. A., & Felser, C. (2021). The topology of electronic band structures. *Nature Materials, 20*(3), 293-300.

Nolen Jr, J., & Schiffer, J. (1969). Coulomb energies. *Annual Review of Nuclear Science, 19*(1), 471-526.

Omboga, N., & Otieno, C. (2020). Structural and electronic properties of the iron pnictide compound EuFe2As2 from first principles. *Journal of Physics Communications, 4*(2), 025007.

Pai, P. F. (1995). A new look at shear correction factors and warping functions of anisotropic laminates. *International Journal of Solids and Structures, 32*(16), 2295-2313.

Panda, K., & Chandran, K. R. (2006). First principles determination of elastic constants and chemical bonding of titanium boride (TiB) on the basis of density functional theory. *Acta Materialia, 54*(6), 1641-1657.

Pang, H., Xu, L., Yan, D.-X., & Li, Z.-M. (2014). Conductive polymer composites with segregated structures. *Progress in Polymer Science, 39*(11), 1908-1933.

Pauli, W. (1994). Exclusion principle and quantum mechanics *Writings on physics and philosophy* (pp. 165-181): Springer.

Phani, K., & Sanyal, D. (2008). The relations between the shear modulus, the bulk modulus and Young's modulus for porous isotropic ceramic materials. *Materials Science and Engineering: A, 490*(1-2), 305-312.

Ran, S., Bud'ko, S. L., Pratt, D., Kreyssig, A., Kim, M., Kramer, M., . . . Roy, B. (2011). Stabilization of an ambient-pressure collapsed tetragonal phase in CaFe 2 As 2 and tuning of the orthorhombic-antiferromagnetic transition temperature by over 70 K via control of nanoscale precipitates. *Physical Review B, 83*(14), 144517.

Reddy, C. M., Krishna, G. R., & Ghosh, S. (2010). Mechanical properties of molecular crystals—applications to crystal engineering. *CrystEngComm, 12*(8), 2296-2314.

Richards, S., Gibbs, R. A., Weinstock, G. M., Brown, S. J., Denell, R., Beeman, R. W., . . . Grimmelikhuijzen, C. (2008). The genome of the model beetle and pest Tribolium castaneum. *Nature, 452*(7190), 949-955.

Rivlin, R. (1948). Large elastic deformations of isotropic materials. I. Fundamental concepts. *Philosophical Transactions of the Royal Society of London. Series A, Mathematical and Physical Sciences, 240*(822), 459-490.

Roby, K. R. (1974). Quantum theory of chemical valence concepts: I. Definition of the charge on an atom in a molecule and of occupation numbers for electron density shared between atoms. *Molecular Physics, 27*(1), 81-104.

Ronning, F., Klimczuk, T., Bauer, E. D., Volz, H., & Thompson, J. D. (2008). Synthesis and properties of CaFe2As2 single crystals. *Journal of physics: Condensed matter, 20*(32), 322201.

Rotter, I. (2003). Effective Hamiltonian and unitarity of the S matrix. *Physical Review E, 68*(1), 016211.

Saha, S., Butch, N., Drye, T., Magill, J., Ziemak, S., Kirshenbaum, K., . . . Paglione, J. (2012). Structural collapse and superconductivity in rare-earth-doped CaFe 2 As 2. *Physical Review B, 85*(2), 024525.

Saha, S. R., Butch, N. P., Kirshenbaum, K., & Paglione, J. (2010). Annealing effects on superconductivity in SrFe2-xNixAs2. *Physica C: Superconductivity and its applications, 470*, S379-S381.

Sakurada, I., Nukushina, Y., & Ito, T. (1962). Experimental determination of the elastic modulus of crystalline regions in oriented polymers. *Journal of polymer science, 57*(165), 651-660.

Samuel, M. V., Otieno, C. O., & Nyawere, P. (2023). Density Functional Study of Mechanical, Electronic and Pressure Induced Phase Transition Properties of CaFé2As2. *Open Journal of Microphysics, 13*(3), 36-51.

Scanlan, R. M., Malozemoff, A. P., & Larbalestier, D. C. (2004). Superconducting materials for large scale applications. *Proceedings of the IEEE, 92*(10), 1639-1654.

Senkpiel, J., Drost, R., Klöckner, J. C., Etzkorn, M., Ankerhold, J., Cuevas, J. C., . . . Ast, C. R. (2022). Extracting transport channel transmissions in scanning tunneling microscopy using superconducting excess current. *Physical Review B, 105*(16), 165401.

Shemansky, D., & Broadfoot, A. (1971). Excitation of N2 and N+ 2 systems by electrons—I. Absolute transition probabilities. *Journal of Quantitative Spectroscopy and Radiative Transfer, 11*(10), 1385-1400.

Shi, G. L., Zhu, S., Bai, S. N., Xia, Y., Lou, L. Q., & Cai, Q. S. (2015). The transportation and accumulation of arsenic, cadmium, and phosphorus in 12 wheat cultivars and their relationships with each other. *Journal of Hazardous Materials, 299*, 94-102.

Siggelkow, L., Hlukhyy, V., & Fässler, T. F. (2010). Synthesis, Structure and Chemical Bonding of CaCo2Si2 and BaCo2Ge2–Two New Compounds with ThCr2Si2 Structure Type: Wiley Online Library.

Silver, A., & Zimmerman, J. (1967). Quantum states and transitions in weakly connected superconducting rings. *Physical Review, 157*(2), 317.

Simon, R. W., Hammond, R. B., Berkowitz, S. J., & Willemsen, B. A. (2004). Superconducting microwave filter systems for cellular telephone base stations. *Proceedings of the IEEE, 92*(10), 1585-1596.

Siryabe, E., Rénier, M., Meziane, A., Galy, J., & Castaings, M. (2017). Apparent anisotropy of adhesive bonds with weak adhesion and non-destructive evaluation of interfacial properties. *Ultrasonics, 79*, 34-51.

Smith, A. M., & Nie, S. (2010). Semiconductor nanocrystals: structure, properties, and band gap engineering. *Accounts of Chemical Research, 43*(2), 190-200.

Stanke, F. E., & Kino, G. S. (1984). A unified theory for elastic wave propagation in polycrystalline materials. *The Journal of the Acoustical Society of America, 75*(3), 665-681.

Sun, L., Chen, X.-J., Guo, J., Gao, P., Huang, Q.-Z., Wang, H., . . . Wu, Q. (2012). Re-emerging superconductivity at 48 kelvin in iron chalcogenides. *Nature, 483*(7387), 67-69.

Toher, C., Plata, J. J., Levy, O., De Jong, M., Asta, M., Nardelli, M. B., & Curtarolo, S. (2014). High-throughput computational screening of thermal conductivity, Debye temperature, and Grüneisen parameter using a quasiharmonic Debye model. *Physical Review B, 90*(17), 174107.

Vitos, L. (2001). Total-energy method based on the exact muffin-tin orbitals theory. *Physical Review B, 64*(1), 014107.

Wagner, E. P. (2016). Investigating bandgap energies, materials, and design of light-emitting diodes. *Journal of Chemical Education, 93*(7), 1289-1298.

Wang, J., Polleux, J., Lim, J., & Dunn, B. (2007). Pseudocapacitive contributions to electrochemical energy storage in TiO2 (anatase) nanoparticles. *The Journal of Physical Chemistry C, 111*(40), 14925-14931.

Wang, Y., Lv, J., Zhu, L., & Ma, Y. (2012). CALYPSO: A method for crystal structure prediction. *Computer Physics Communications, 183*(10), 2063-2070.

Wannier, G. H. (1937). The structure of electronic excitation levels in insulating crystals. *Physical Review, 52*(3), 191.

Winichayakul, S., Beechey-Gradwell, Z., Muetzel, S., Molano, G., Crowther, T., Lewis, S., . . . Roberts, N. (2020). In vitro gas production and rumen fermentation profile of fresh and ensiled genetically modified high–metabolizable energy ryegrass. *Journal of Dairy Science, 103*(3), 2405-2418.

Woodward, R. B., & Hoffmann, R. (1969). The conservation of orbital symmetry. *Angewandte Chemie International Edition in English, 8*(11), 781-853.

Yang, Y., Yu, H., York, D., Cui, Q., & Elstner, M. (2007). Extension of the self-consistent-charge density-functional tight-binding method: third-order expansion of the density functional theory total energy and introduction of a modified effective coulomb interaction. *The Journal of Physical Chemistry A, 111*(42), 10861-10873.

Yin, Z. P., Haule, K., & Kotliar, G. (2014). Spin dynamics and orbital-antiphase pairing symmetry in iron-based superconductors. *Nature Physics, 10*(11), 845-850.

Yoffe, A. D. (2001). Semiconductor quantum dots and related systems: electronic, optical, luminescence and related properties of low dimensional systems. *Advances in physics, 50*(1), 1-208.

Zhang, R., & Deng, C. (1993). Exact solutions of the Schrödinger equation for some quantum-mechanical many-body systems. *Physical Review A, 47*(1), 71.

Zunger, A., & Freeman, A. (1977). Self-consistent numerical-basis-set linear-combination-of-atomic-orbitals model for the study of solids in the local density formalism. *Physical Review B, 15*(10), 4716.

APPENDIX I: CONFERENCE

DENSITY FUNCTIONAL STUDY OF MECHANICAL, ELECTRONIC AND PRESSURE INDUCED PHASE TRANSITION PROPERTIES OF CALCIUM DIIRON DIARSENIDE, $CaFe_2As_2$

MOCHAMA VICTOR SAMUEL

SUPERVISORS

DR. CALFORD OTIENO
DR. P.W.O NYAWERE

APPENDIX II: PUBLICATION

Scientific
Research
Publishing

Density Functional Study of Mechanical, Electronic and Pressure Induced Phase Transition Properties of CaFe$_2$As$_2$

Mochama Victor Samuel[1], Calford Odhiambo Otieno[1], Phillip Nyawere[2]

[1]Department of Physics, Kisii University, Kisii, Kenya
[2]Department of Physical and Biological Sciences, Kabarak University, Nakuru, Kenya
Email: mochamavic@gmail.com

Abstract

We report results on the *ab initio* study of the mechanical and electronic properties of the iron Pnictide compound CaFe$_2$As$_2$ and its phase transition under pressure using Quantum Espresso code. We do analysis of the strength of bonds in individual points of this material and proper Cauchy pressure calculation which will give more insight on the elastic responses. Ground state energy was done in the framework of density functional theory (DFT) based on plane wave self-consistent field (PWscf) and ultrasoft pseudo potential (USPP) method as treated in the Perdew-Burke Ernzerhof (PBE) generalized gradient approximation and local density approximations. Elastic constants were computed using thermo_pw and the values were used to calculate mechanical properties and pressure phase changes. From the non-zero positive elastic constants, the Iron Pnictide compound is found to be mechanically stable and its Poisson's ratio indicates that it is brittle and isotropic. Pressure induced phase transition is here found to happen at an applied external pressure of 0.2 GPa causing the tetragonal phase to change to an orthorhombic phase which agrees well with previous reports.

Keywords

Phase Transition, Elastic Constants, Modulus

APPENDIX III: INPUT FILE

This is a self-Consistent input file for the material under study.

&control

  calculation = 'scf'

  restart_mode='from_scratch',

  outdir = './tmp/'

  prefix = 'CaFe2As2'

  pseudo_dir = './'

/

&system

 ibrav=7,

 celldm(1) =7.89635

 celldm(3) = 3.23425

 nat= 5,

 ntyp= 3

 nbnd= 52

 ecutwfc= 40

 ecutrho= 410.5

 occupations= 'smearing'

 smearing= 'gaussian'

 degauss= 0.01

 /

&electrons

conv_thr =   1.0d-8

mixing_beta =   0.2

/

ATOMIC_SPECIES

As   74.9216 As.pbe-n-kjpaw_psl.1.0.0.UPF

Ca   40.078 Ca_pbe_v1.uspp.F.UPF

Fe   55.847 Fe.pbe-spn-kjpaw_psl.0.2.1.UPF

ATOMIC_POSITIONS (crystal)

As   0.438180441   0.347038371 -0.091142070

As   0.561819559   0.652961629   0.091142070
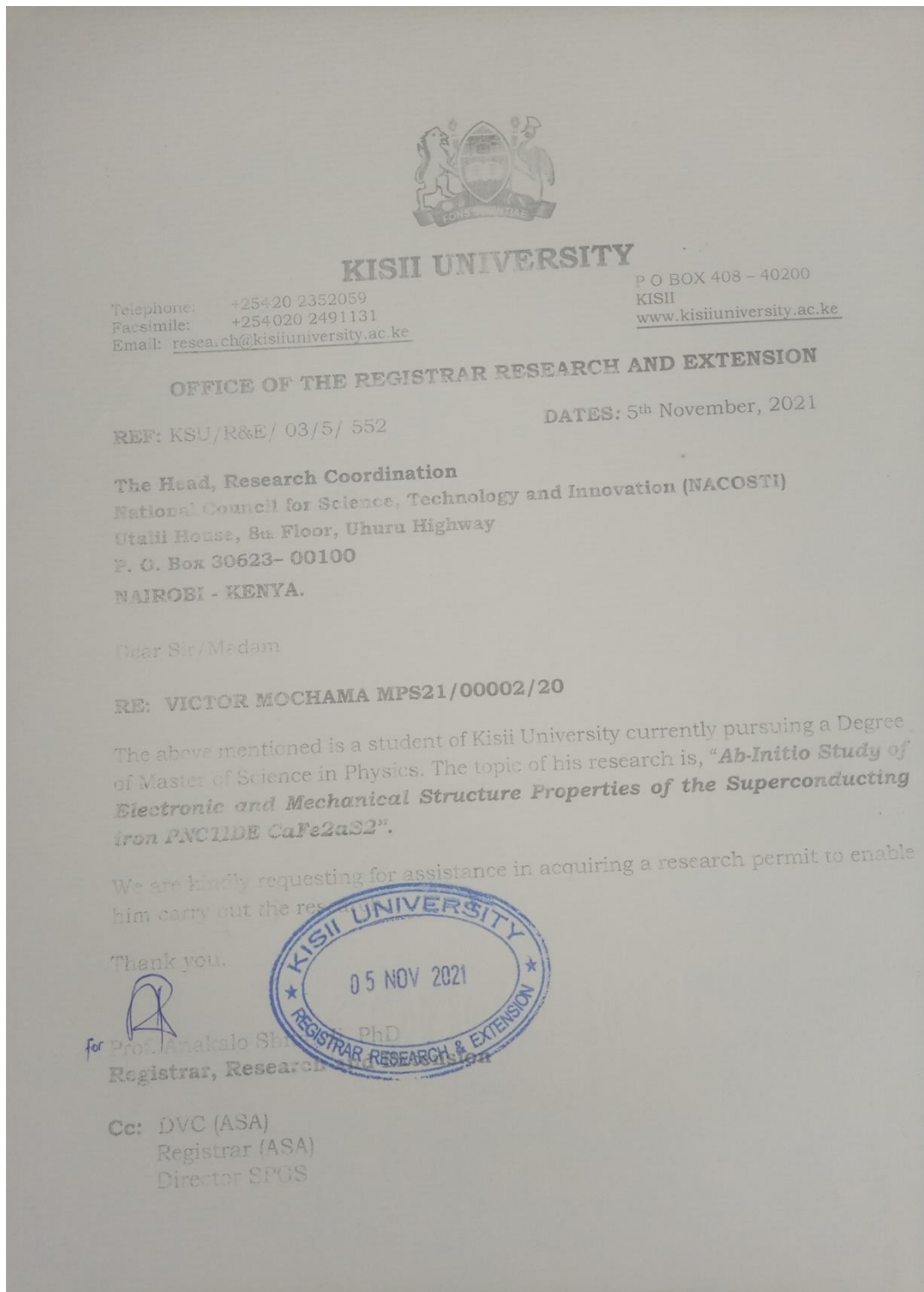
Ca   0.000000000 -0.000000000 -0.000000000

Fe   0.056396927   0.751633072   0.695236145

Fe   0.943603073   0.248366928   0.304763855

K_POINTS automatic

 6 6 4 0 0 0

APPENDIX IV: INTRODUCTION LETTER

KISII UNIVERSITY

P O BOX 408 – 40200
KISII
www.kisiiuniversity.ac.ke

Telephone: +254 20 2352059
Facsimile: +254 020 2491131
Email: resea.ch@kisiiuniversity.ac.ke

OFFICE OF THE REGISTRAR RESEARCH AND EXTENSION

REF: KSU/R&E/ 03/5/ 552

DATES: 5th November, 2021

The Head, Research Coordination
National Council for Science, Technology and Innovation (NACOSTI)
Utalii House, 8th Floor, Uhuru Highway
P. O. Box 30623– 00100
NAIROBI - KENYA.

Dear Sir/Madam

RE: VICTOR MOCHAMA MPS21/00002/20

The above mentioned is a student of Kisii University currently pursuing a Degree of Master of Science in Physics. The topic of his research is, *"Ab-Initio Study of Electronic and Mechanical Structure Properties of the Superconducting Iron PNCTIDE CaFe2aS2"*.

We are kindly requesting for assistance in acquiring a research permit to enable him carry out the research.

Thank you.

for Prof. Anakalo Sh... PhD
Registrar, Research...

0 5 NOV 2021
KISII UNIVERSITY
REGISTRAR RESEARCH & EXTENSION

Cc: DVC (ASA)
    Registrar (ASA)
    Director SPGS

84

APPENDIX V: NACOSTI PERMIT

This Research got permission from National Commission for Science, Technology and Innovation.

REPUBLIC OF KENYA

NATIONAL COMMISSION FOR SCIENCE, TECHNOLOGY & INNOVATION

Ref No: 679080

Date of Issue: 03/December/2021

RESEARCH LICENSE

This is to Certify that Mr.. Mochama Victor Samuel of Kisii University, has been licensed to conduct research in Kisii on the topic: AB-INITIO STUDY OF ELECTRONIC AND MECHANICAL STRUCTURE PROPERTIES OF THE SUPERCONDUCTING IRON PNICTIDE for the period ending : 03/December/2022.

License No: NACOSTI/P/21/14712

679080

Applicant Identification Number

Director General
NATIONAL COMMISSION FOR SCIENCE,TECHNOLOGY & INNOVATION

Verification QR Code

NOTE: This is a computer generated License. To verify the authenticity of this document,
Scan the QR Code using QR scanner application.

APPENDIX VI: PLAGIARISM REPORT

DENSITY FUNCTIONAL STUDY OF MECHANICAL, ELECTRONIC AND PRESSURE INDUCED PHASE TRANSITION PROPERTIES OF CALCIUM DIIRON DIARSENIDE, CaFe 2 As 2

ORIGINALITY REPORT

19%	15%	11%	6%
SIMILARITY INDEX	INTERNET SOURCES	PUBLICATIONS	STUDENT PAPERS

PRIMARY SOURCES

1	**Submitted to Kisii University** Student Paper	2%
2	www.researchgate.net Internet Source	1%
3	erepository.kafuco.ac.ke Internet Source	1%
4	arxiv.org Internet Source	1%
5	library.kisiiuniversity.ac.ke:8080 Internet Source	1%
6	www.coursehero.com Internet Source	1%
7	Submitted to Visvesvaraya National Institute of Technology Student Paper	1%
8	ebin.pub Internet Source	<1%